Temperature Measurement Using Rare-Earth Spectra

A Major Qualifying Project Report:

Submitted to the Faculty of the

WORCESTER POLYTECHNIC INSTITUTE

In partial fulfillment of the requirements for the

Degree of Bachelor of Science

by

Brian Foley
April 24, 2008

Approval:

Richard Quimby, Advisor

Abstract

The goal of this project was to determine how precisely temperature can be measured using rare-earth ion spectra, and to determine the Stark levels of the rare earth ion multiplets. The absorption spectra of Er-doped silicate glass were studied, and a method was developed to determine temperature change. Emission spectra were used and was calculated from the absorption spectrum by the McCumber method. An uncertainty in temperature of approximately ±10K was obtained, and a simplified Stark level model was constructed.

Table of Contents

Introduction

The following paper goes into detail in using the absorption and emission spectra of rare-earth elements to determine temperature. In such experiments, thermometers or thermocouples could be used to record temperature. However, in some applications, these methods could be detrimental to the experiment. Thermometers and thermocouples are invasive methods and may affect the results. Also, non-contact ways exist to measure temperature change involving blackbody radiation. This is because blackbody radiation depends on temperature as stated by Wein's displacement law.[1]

$$T\lambda_{\max} = 2.898 * 10^{6} \text{ nm K} \quad (1)$$

However the blackbody spectrum is very broad and not applicable in certain situations to measure temperature. Because of this, the absorption and emission spectra of rare-earth elements will be studied to determine a temperature change. The goal of our experiment was to find the uncertainty of temperature change and determine the existing Stark levels of the rare-earth spectra.

Background

Rare-Earth Elements

Before starting the experiment, a basic understanding of important concepts on the subject was crucial. The rare-earths are broken into two groups; the first group is the lanthanides, and the second group is the actinides. The lanthanides fill the 4*f* shell and range from atomic numbers 58 to 71, while the actinides fill the 5*f* shell and range from

atomic numbers 90-103. It is also important in understanding the quantum numbers associated with rare-earth elements. The quantum numbers are L, S, and J, where L is the total orbital angular momentum, S is the total spin, and J is the total angular momentum. The notation for quantum numbers is $^{2S+1}L_J$. The total orbital angular momentum is specified by letters S, P, D, F, G, H, I, K which are represented by L= 0,1,2,3,4,5,6,7 respectively.[2]

The lanthanides and actinides experience special properties that are fundamental to understand before conducting the experiment. One is the phenomenon of electron shielding. Electron shielding occurs when the 5*s* and the 5*p* orbital are filled with electrons; however the 4*f* shell has not been completely filled. The 5*s* and 5*p* orbitals act as a shield, causing the 4*f* shell electrons to interact very weakly with surrounding ions.[3]

Another important property these elements experience is known as Stark splitting. This can be viewed in Figure 1.

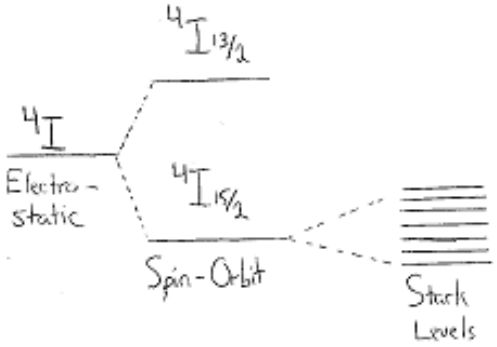

Figure 1: The different splitting interactions found for atoms

The splitting occurs when the presence of an electric field causes the splitting of spectral lines of atoms and molecules. This is known as the Stark effect. This then causes the energy manifolds to be separated into sub-energy levels. Therefore, instead of emission and absorption only occurring between the energy manifolds, the individual Stark levels will experience these transitions.[2]

Another important factor to understand is the different types of transitions that may occur. This comes in the form of radiative and nonradiative transitions. There are three types of radiative transitions, spontaneous emission, absorption, and stimulated emission. Spontaneous emission can be seen in Figure 2.

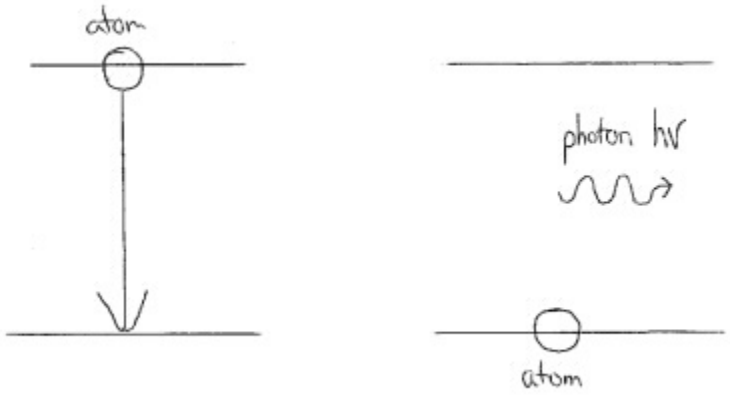

Figure 2: Spontaneous emission of an atom

Figure 2 shows an atom in the excited states moving to the ground state. The figure also shows that once the process is completed a photon is emitted after the emission. If this were the only type of radiative transition, all excited state levels would always decay to the ground state. However thermal equilibrium proves that this is not the case, shown by the Boltzmann factor. The Boltzmann factor equation is[4]

$$\frac{N_2}{N_1} = e^{-E_{21}/(kT)} \qquad (2)$$

Where N_2 is the number of atoms in level 2, N_1 is the number of atoms in level 1, E_{21} is the energy difference between the two levels, k is the Boltzmann constant and T is the absolute temperature. Equation 2 proves atoms will exist in an excited state as long as the temperature is greater than absolute zero.

When atoms are in the excited state, there needs to be a radiative transition known as absorption. Absorption is seen in Figure 3 and shows an incoming photon being absorbed therefore moving the atom from level 1 to an excited state (level 2 in this case).[5]

Figure 3: Absorption of an atom

The final type of radiative transition is stimulated emission. Figure 4 shows an example, where an atom in the excited state and incoming photon (photon 1) interact.

Figure 4: Stimulated Emission of an atom

As photon 1 passes through, the atom in the excited state decays to the ground state, releasing another photon (photon 2) with the same energy of the energy gap between the two states and photon 1.[5]

In our experiment, radiative transitions are needed to provide reliable data. However, nonradiative transitions have a negative impact on the results. Nonradiative transitions are observed when conducting an experiment with a rare-earth element doped in a type of solid. When a rare-earth is doped in a solid, vibrations occur between the rare-earth and its host material. These solid vibrations correspond to the emission of phonons. A unique property that phonons acquire is in many cases one single phonon does not have enough energy to bridge the energy gap. However, phonons have the property where energy of multiple phonons is able to bridge the energy gap if the energy of one phonon is not enough. To avoid phonon interactions from predominately occurring, the energy between the levels needs to be greater than the energy of the phonons. More phonons are then required to bridge the energy gap. When radiative and

nonradiative transitions are comparable, the efficiency of the absorption/emission process is degraded.[6]

In addition, there are a number of equations important to understand the rare-earth spectra. Equations 3 and 4 will be used to manipulate the raw data that is obtained into usable data for the analysis. The first equation needed is Beer's Law.[3]

$$\frac{I_1}{I_0} = e^{-\alpha l} \tag{3}$$

where I_1 is the intensity of light with a sample in the path of the beam, I_0 is the intensity of light with sample removed from the path of the beam, α is the absorption coefficient, and l is the length needed for the beam to travel through the sample. In our experiment, the sample used is erbium doped in a glass (Er:L22). A halogen tungsten lamp produces the light source. Equation 3 provides a solution for α since the other variables can be obtained from the experiment.

After calculating the absorption coefficient, it is possible to determine the absorption cross section from the following equation[3]

$$\sigma_a = \frac{\alpha}{N} \tag{4}$$

Where σ_a is the absorption cross section, α is the absorption coefficient, and N is the number of ions in the sample per unit volume. The absorption cross section allowed us to compare other absorption cross sections of various temperatures, resulting in observing how the spectra of rare-earth elements changed with temperature.

A final important relationship involved the absorption cross section and its relationship to the emission cross section. The emission cross section is able to be determined experimentally; however there is also a method to determine it theoretically if

the absorption cross section is known. This allows time to be saved and is a fairly accurate representation of the emission spectrum. The equation used is the McCumber relation and is[7]

$$\sigma_e(\lambda) = \sigma_a(\lambda) e^{\frac{hc}{\lambda_0} - \frac{hc}{\lambda}} \quad (5)$$

Where $\sigma_e(\lambda)$ is the emission cross section, $\sigma_a(\lambda)$ is the absorption cross section, h is Planck's constant, c is the speed of light, λ_0 is a constant wavelength chosen, and λ is the different wavelengths over the entire spectrum. Equation 5 shows that the absorption spectrum for wavelengths longer than λ_0 is amplified, while the absorption for shorter wavelengths λ_0 is diminished. This produces an accurate representation of the emission cross section when compared experimentally and has been proven in past research.[7]

Literary Review

After preliminary background research, various scientific journals were searched to gain an understanding on work that was accomplished on the topic. Various articles already were published on the relationship between rare-earth emission and absorption spectra and the relationship to temperature. One of the useful papers was by Nikonorov.[8] The experiment conducted relied on the fluorescence and absorption spectra of Er-doped in phosphate and silicate glasses. These samples are similar to the one tested in our experiment. The temperature range being investigated was between 20-300°C. The motivation in conducting this experiment was to observe how the absorption and emission spectra change with temperature and to suggest a plausible explanation for this occurrence. The conclusion was the absorption and emission spectra did vary with

temperature. This observation was explained by the Stark sub-levels, as shown in Figure 5. For the erbium doped in a phosphate glass, the paper observed two transitions at 1534 and 1542nm. An older simplified model for these transitions (Figure 5a) proved to be inaccurate, and so an updated model was developed. The new model (Figure 5b) replaced the upper manifold with two Stark levels, and the lower manifold with two Stark levels. From the model the Stark levels were able to be determined and were 50cm^{-1} and 100cm^{-1} for the $^4I_{13/2}$ and the $^4I_{15/2}$.[8]

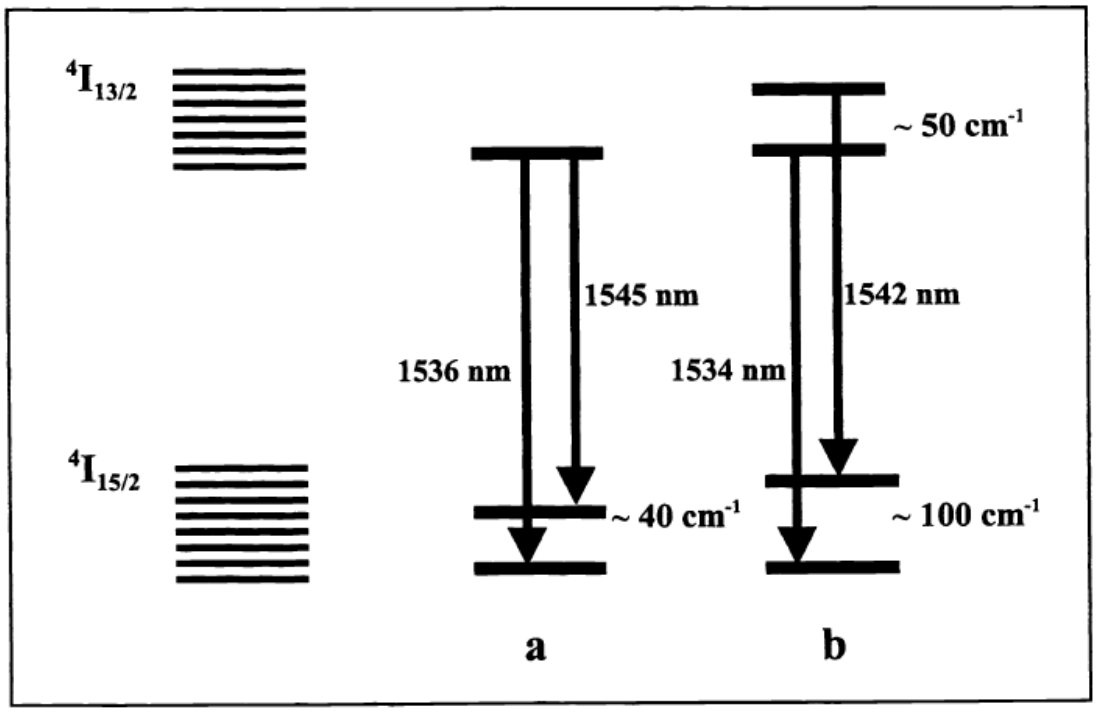

Figure 5: Stark level model of Er-doped phosphate glass (a)model of Kuchma (b) new model (Taken From Nikonorov)[8]

The next paper examined was by Zemon.[9] The paper focused on relevant information of the energies in the Stark levels. A problem that was presented in Zemon's paper was homogeneous and inhomogeneous broadening in emission and absorption

spectra.[9] In order to account for homogeneous broadening, very low temperatures were used to eliminate the vibrations of the solids. For the inhomogeneous broadening, fluorescence line narrowing was used. After using these methods and looking at a number of samples the Stark levels were determined for $^4I_{15/2}$ and $^4I_{13/2}$.[9] Figure 6 shows an example of their model.

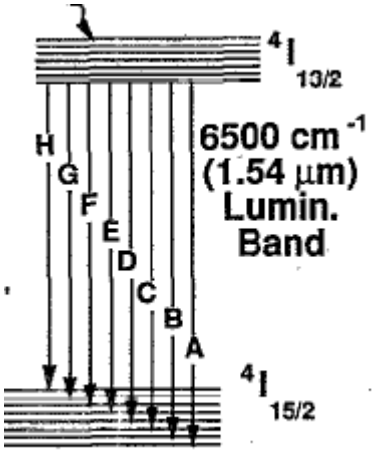

Figure 6: Energy level diagram at 4.2 K for luminescence transitions between of $^4I_{13/2}$ and of $^4I_{15/2}$ due to laser pumping. (Taken from Zemon)[9]

From Figure 6 the letter represent transition peaks where A is the shortest wavelength and H is the longest wavelength. Another interesting figure presented in Zemon's paper was the analysis of Stark energy levels of $^4I_{15/2}$ and their energy in cm^{-1}. The photon energy can be expressed as a reciprocal wavelength according to[1]

$$E(\lambda) = \frac{hc}{\lambda} \propto \frac{1}{\lambda} \qquad (6)$$

Where E is the photon energy at a particular wavelength, h is Planck's constant, c is the speed of light, and λ is the wavelength. The conversion factor between cm^{-1} and electron volts is $1cm^{-1}$ is $1.23*10^{-4}$ eV. A chart of the transition energies can be viewed in Figure 7.

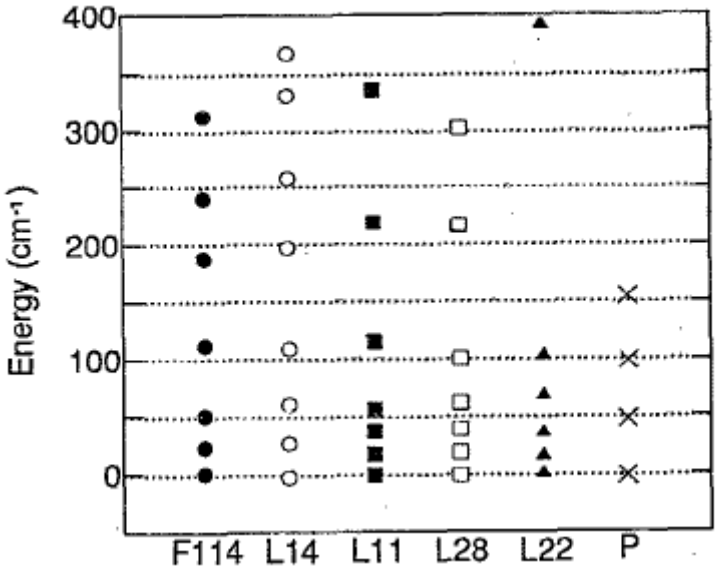

Figure 7: Comparison of Stark energy levels of $^4I_{15/2}$ for a number of different samples. L22 was the sample used in our experiment. (Taken from Zemon)[9]

The information from Figure 7 could prove useful when constructing the Stark level model.

Another paper examined was by Koroshez.[10] This paper examined how the emission cross-section changed with temperature. The method of obtaining the emission cross-section was similar to the approach we will use. First Koroshetz took the absorption spectrum for Yb,Er: phosphate glass, then used the McCumber relation (Eq. 5) to produce an emission cross section. The graph that was produced from his experiment can be seen in figure 8.[10]

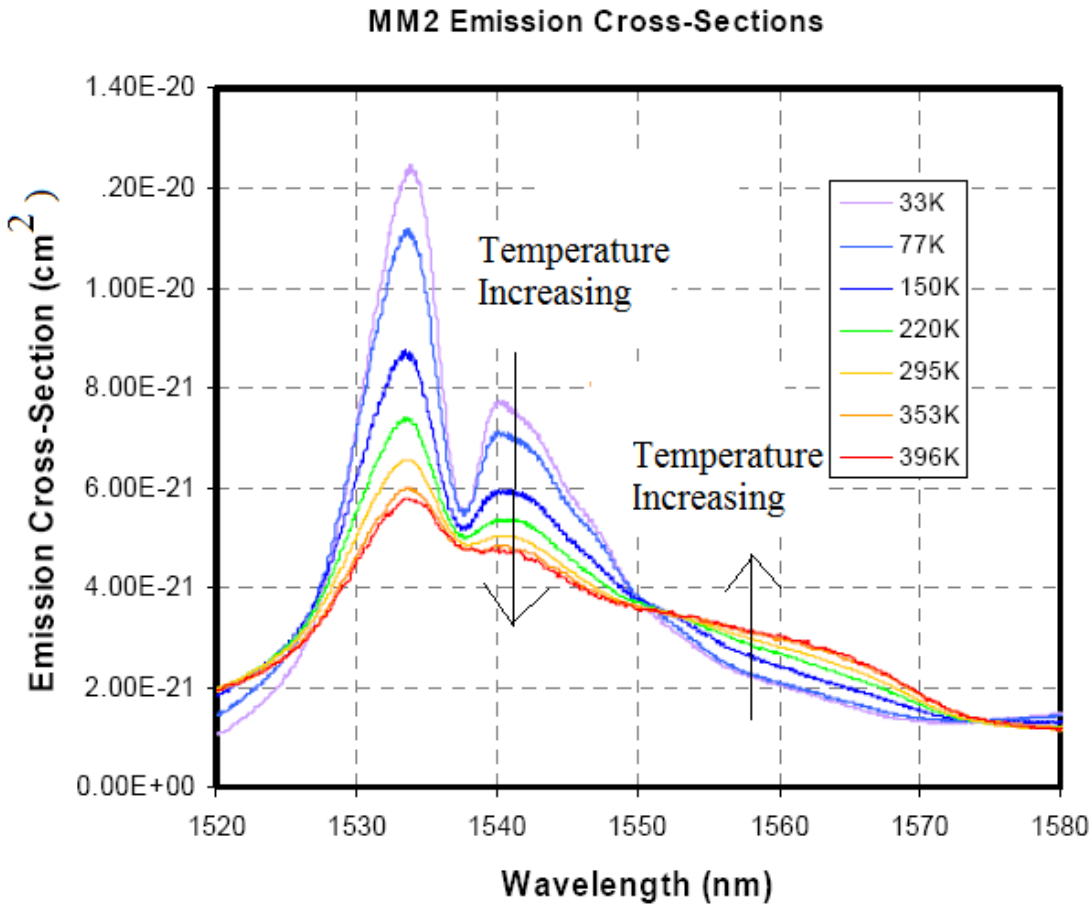

Figure 8 : Emission Cross-Section varying with temperature (Taken Directly from Koroshetz)[10]

Figure 8 shows there is a noticeable change as the temperature changes over the temperature interval. One of the important features of the graph is that at 1534nm and 1541nm, when the temperature increases the emission cross-section decreases. However, around 1560nm as the temperature increases the emission cross-section also increases. We expect to see a change similar to Koroshetz.[10]

Experimental Setup and Procedure

Experimental Setup

For the experimental part of the experiment, it was necessary to have equipment suitable to scan through a range of wavelengths 1200-1800 nm. The light source for the experiments was a halogen tungsten lamp. The lamp was set to a constant current value of 3 ampere which corresponded to a voltage of 5.45-5.46 Volts. In order to collect the light from the halogen tungsten lamp, a set of lens were used. To determine the positioning of the lens it was necessary to use equation 7 to find their focal lengths[3]

$$\frac{1}{f} = \frac{1}{s} + \frac{1}{s'} \tag{7}$$

where f is the focal length, s is the distance from the light source to lens, and s' is the distance from the lens to the image. The focal length for the lenses used was approximately 5cm. By knowing the focal length, the lens was positioned beyond 5cm to allow the light to form a small point that would allow the beam to entirely travel through the sample. Next, a chopping wheel was required to send a reference signal to the lock-in amplifier. The chopping wheel was set at a frequency of 80Hz in order for there to be no fluctuation in the data at a single wavelength. Another lens was then needed to collect the light and have the beam pass through a 950nm long pass filter. A long-pass filter acts as a cutoff that transmits longer wavelengths and blocks shorter wavelengths. The reason the beam is needed to pass through a filter is to eliminate any second order spectra. Second order spectra occur at wavelengths approximately half the wavelength being testing in the scanning spectrometer. For example, when measuring a signal at 1600nm, signal of a second order spectrum may occur because of the 800nm photons.

In our experiment a filter of cutoff wavelength 950nm was used. Since the wavelength interval was from 1200-1800nm, this eliminated any present second order spectrum. After passing through the filter the beam entered a scanning spectrometer to record data for various wavelengths. The speed of the scanning spectrometer was set to 50nm/min. At the exit slit of the scanning spectrometer an InGaAs photon detector was placed and was connected to the lock-in amplifier also. The lock-in amplifier settings were a time constant of 1 second and a sensitivity of 250mV. The data was sent to a computer, where it was saved and stored. The data interval was 0.5nm. If the scanning speed was increased or data interval decreased, an anomaly in the data software occurred. The actual set up of the experiment can be seen in figure 9.

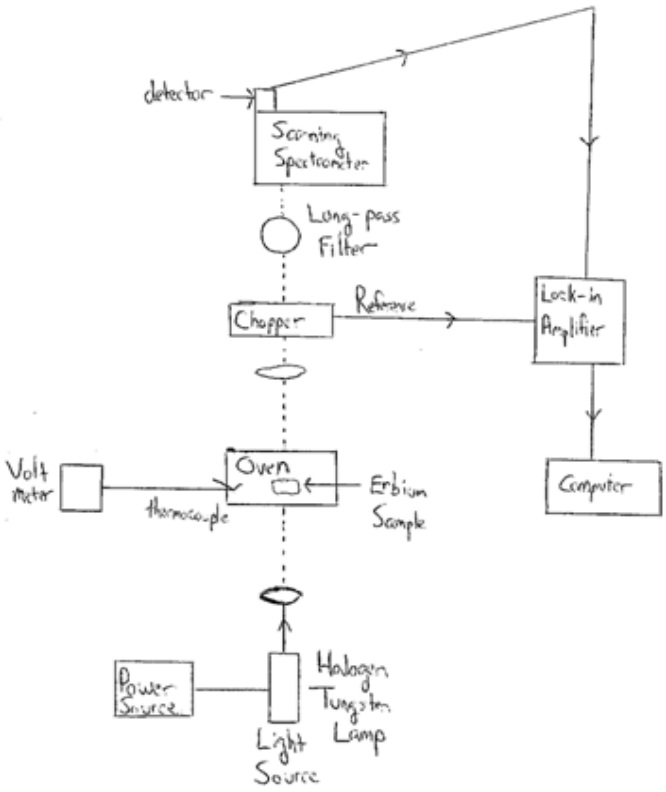

Figure 9: Experimental setup for absorption measurements

Preliminary Experiments

With the experiment set-up, a few preliminary experiments were done to determine values for the entrance slit width and exit slit width, as well was what peak width was required to successfully see accurate peak structure. First the experiment was run to see what peak width would be needed in order to see structure. To accomplish this task the same experimental setup was used as in Figure 9, but instead of a halogen tungsten lamp, a helium neon laser was used. With a helium neon laser an infinitely

narrow peak is expected at 632.8nm. The results of this experiment can be seen in Figure 10.

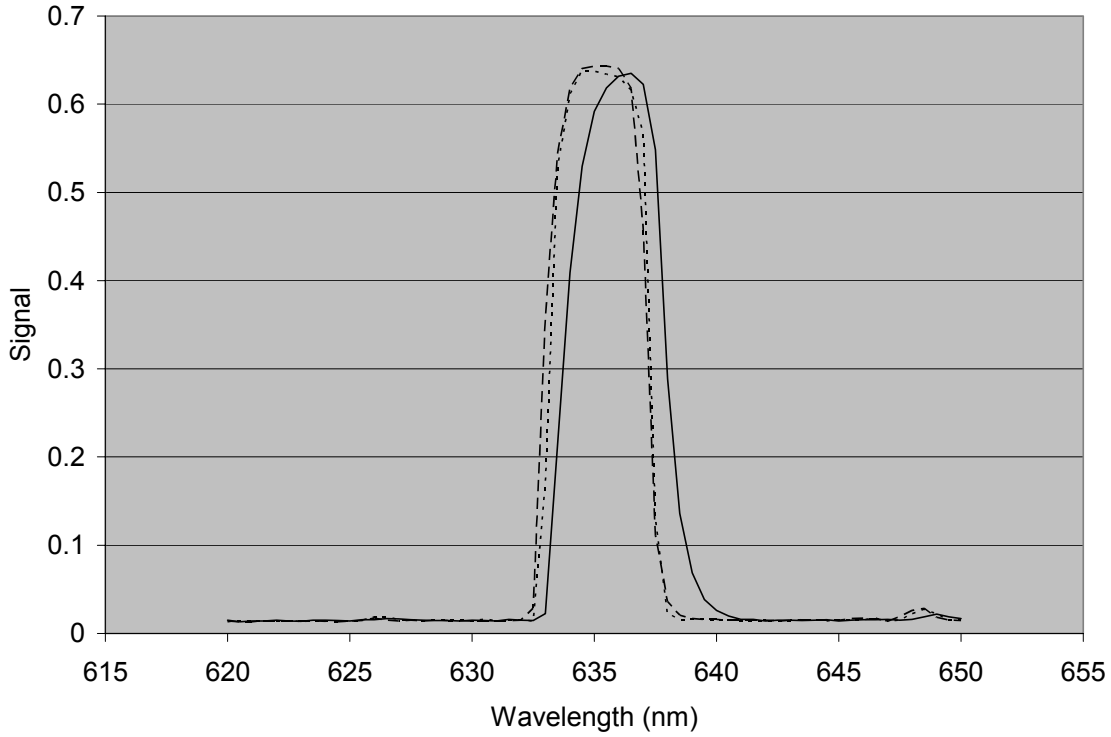

Figure 10: Testing scanning spectrometer for necessary scan-speed to observe accurate data, dashed line (25nm/min), dotted line (50nm/min), solid line (100nm/min) at slit-width of 0.6mm

From figure 10, the dashed line represented a scanning speed of 25nm/min with remaining settings being held constant (time constant (tc)=.3s, sensitivity: 100mV, wavelength interval 0.2nm) , the dotted line represented a scanning speed of 50nm/min, and solid line represented 100nm/min. Figure 10 allows one to see that the helium neon laser is able to see the peak begin around 632-633nm, however it is not infinitely narrow, instead has peak width of approximately 5nm. Also Figure 10 showed the optimal

scanning speed for our experiment. For scanning speeds of 25nm/min and 50nm/min the results of the experiment were similar. But for the scanning speed of 100nm/min, the data began to shift to longer wavelengths. This observation does agree because of the value of our time constant, 0.3 seconds. The theoretical wavelength shift with a scanning speed of 100nm/min and a time constant of 0.3 seconds is 0.5nm. The experimental wavelength shift was 0.57nm (Figure 10). The shift in the data is attributed to fast scanning speeds and slower time constants causing a shift in the data to longer wavelengths. We concluded that a scanning speed of 50nm/min would be acceptable because it provided the fastest scanning speed with the data not beginning to shift towards longer wavelengths. The following preliminary experiment shows that we want at least a width of 5nm for the peaks found and a scanning speed of 50nm/min, otherwise the data may be affected by the resolution and scanning speed of the scanning spectrometer.

Next an appropriate sample had to be chosen that would provide adequate peak structure (multiple well defined peaks). The rare-earth chosen to use was Erbium. The reason for choosing the sample of erbium is because the amount of research conducted with the sample in the past, as well as textbooks which provided example absorption and emission spectra of this rare-earth. The first erbium tested was Er:ZBLAN and did provide two well defined peaks between the wavelengths of 1450-1600nm for the absorption spectrum; however sources did not show an as strong peak structure for the emission spectrum. Another sample was then tested, Er:L22 in a silicate glass. An absorption spectrum can be seen in figure 11, and there are four well defined peaks for the absorption spectrum. It was decided to use Er:L22 for the sample to be tested.

The next preliminary experiment was to test various slit-widths and how they would affect the resolution of the scanning spectrometer. Slit-widths of 0.2, 0.3, 0.4, 0.5, 0.6, and 0.7mm were used in an experimental setup as seen previously in figure 9. Scans using the setup with a sample in and out of the beam were conducted and the absorption cross section was calculated. An example of an absorption cross section can be found in figure 11.

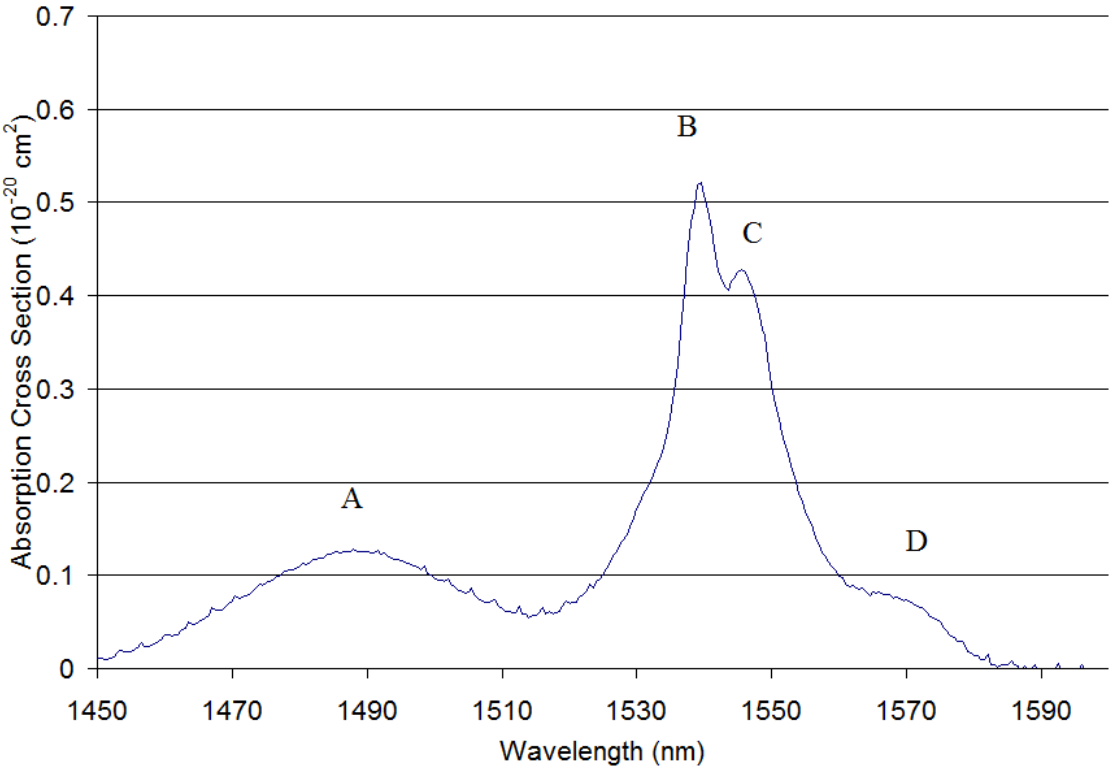

Figure 11: Labeled peaks A, B, C, and D for reference in the paper: Er:silicate sample

In figure 11, there are four distinct peaks that can be seen labeled respectively A, B, C, D. Their wavelengths and energies are in Table 1.

Peak	wavelength (nm)	energy (cm^{-1})
A	1494	6693
B	1539	6498
C	1545	6472
D	1566	6386

Table 1: Peak heights with their wavelength and energy (Absorption)

The ratio of peak heights B and C were compared for the slit widths listed above. The reason the ratio of peaks was compared because as the slit width increases, the two peaks would broaden and blend together, the ratio approaching unity. For the best signal-to-noise ratio the greatest slit width should be used to allow the most amount of signal into the scanning spectrometer while keeping a defined peak structure. After the data was recorded it was able to be plotted and can be seen in figure 12.

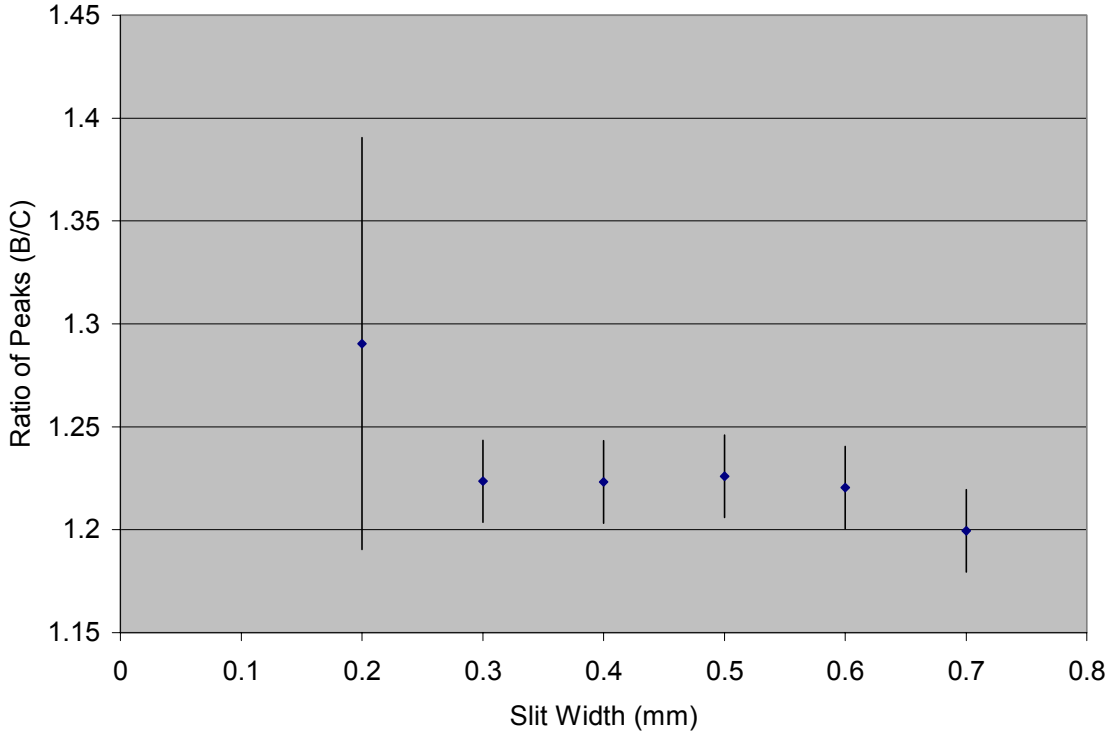

Figure 12: Determining necessary slit-width for experiment with ratio of peak heights B/C

Figure 12 shows the ratio is approximately constant between the slit widths 0.3-0.6mm, however at 0.7mm it is observed that the structure of the two peaks becomes less defined. Therefore a slit width of 0.6mm was used for the entrance and exit slit widths since it would allow the most light into the scanning spectrometer and keep a defined shape of the peaks.

With the preliminary experiments finished, the final experiment setup was now finalized and remained throughout the experiment. The setup can be seen in Figure 9. First, a halogen tungsten lamp, driven with a current of 3 ampere, provided light that was collected by a lens with focal length 5cm. The beam then passed through an oven where Er:L22 would be located. Within the oven, a thermocouple (made of copper-constantan)

was placed in the air to measure the increase of oven temperature. Data from the thermocouple could be recorded from a voltmeter once the reading became constant. Next another lens, with focal length 5cm, collected the light and then passed the beam through a chopping wheel set at a frequency of 80 Hertz. Then the beam of light passed through a 950nm long-pass filter and entered a scanning spectrometer through the 0.6mm slit. Data is then recorded from a wavelength range of 1200-1800nm with a scanning speed of 50nm/min. The light exits the scanning spectrometer through a 0.6mm slit and the amplified InGaAs photon detector connected to the lock-in amplifier records the data at a time constant of 1 second and a sensitivity of 250mV. This procedure for the experiment was repeated twice, once without the sample and once with the sample in the path of the beam.

Experimental Results

Results

With a finalized procedure, it was now possible to begin to obtain raw data with the sample in and out the path of the beam. However, certain steps were needed to obtain useable data in order to make an analysis of the readings. Here are the steps that need to be taken before comparing the ratio of peak heights and how they vary over temperature. For the following absorption spectrum, the temperature remained constant at 300K. Figure 13 and figure 14 are two examples of the raw data for the sample out and sample in the beam respectively.

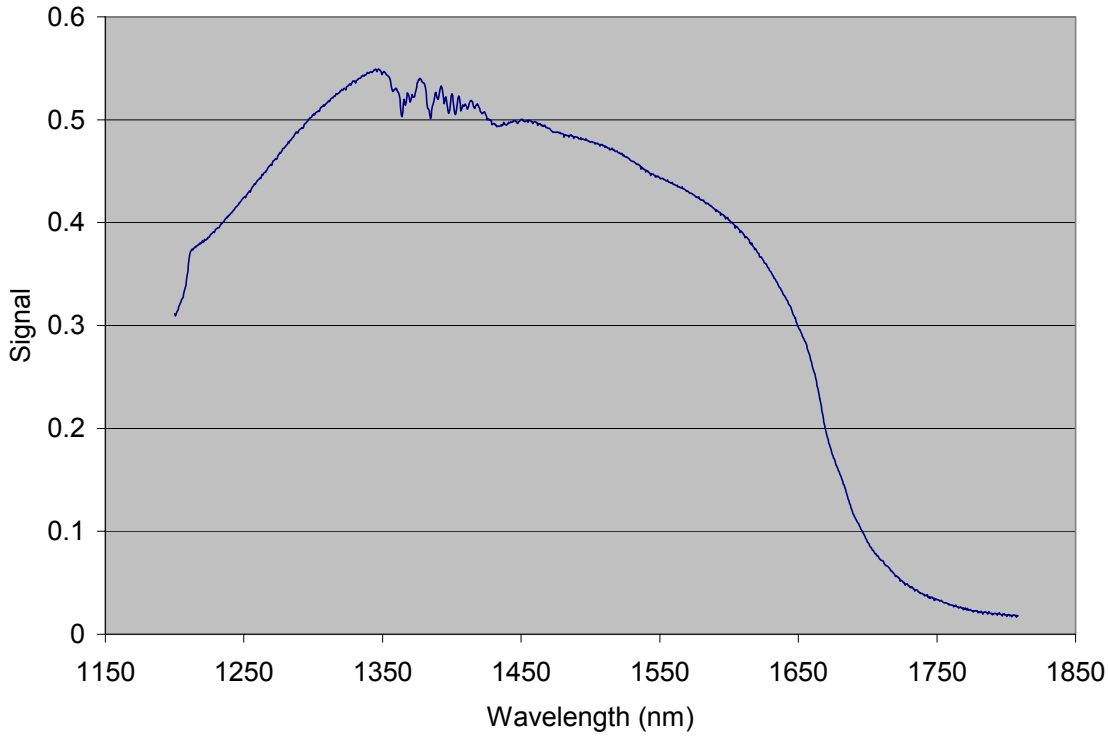

Figure 13: Raw data with no sample, Er:silicate glass, in the path of the beam at room temperature

Figure 14: Raw data with the sample, Er:silicate glass, in the path of the beam at room temperature

As can be seen in figures 13 and 14, around 1350nm to 1400nm there is a fluctuation in data. This can be attributed to the light being absorbed by water vapor at these wavelengths. However in the next step you will see that this fluctuation in signal will be cancelled out with each other. To calculate the absorption spectrum, Beer's Law is used, which is found in equation (3). Using the graphs for the sample in and out the path of the beam we take the natural log of the ratio of these values, resulting in

$$\alpha \propto \ln \frac{I_0}{I_1} \tag{8}$$

Where α is the absorption coefficient, I_0 is the intensity of light with the sample out of the path of the beam, and I_1 is the intensity of light with the sample in the path of the beam.

This relationship results in figure 15 which is the log of the ratio over the wavelength range.

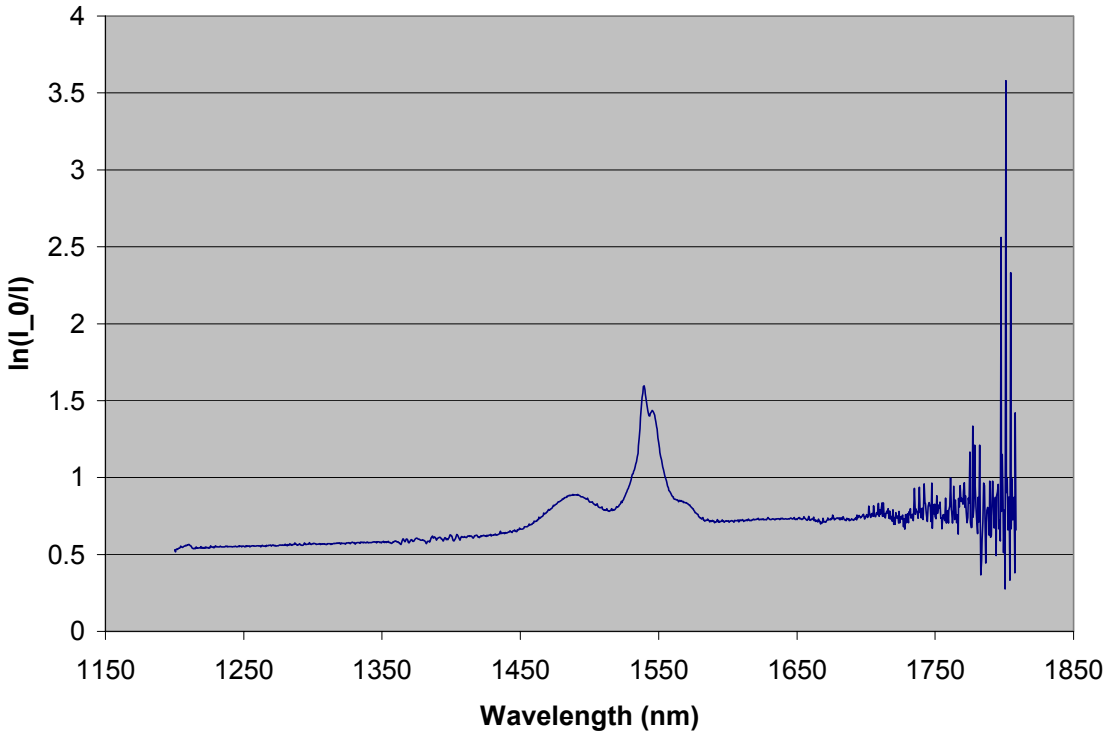

Figure 15: Natural log of the ratio between sample out of the path of the beam and sample in the path of the beam

In figure 15 the data has not yet been normalized. In order to do so a best fit line needs to be plotted for the base-line. At wavelengths shorter than 1450nm and longer than 1600nm, the absorption cross-section should equal zero. To accomplish this, a quadratic fit was used for the wavelengths around the two mentioned above. However it is important to not include wavelengths at the beginning and end of the spectrum. If these wavelengths are included, the signal to noise ration will have an effect on the results because of the noise present at the longer wavelengths. Including the shortest and longest

wavelengths, the quadratic fit would not normalize the absorption spectrum at the range desired. Figure 16 shows an example of how the best-fit line was obtained from Figure 12.

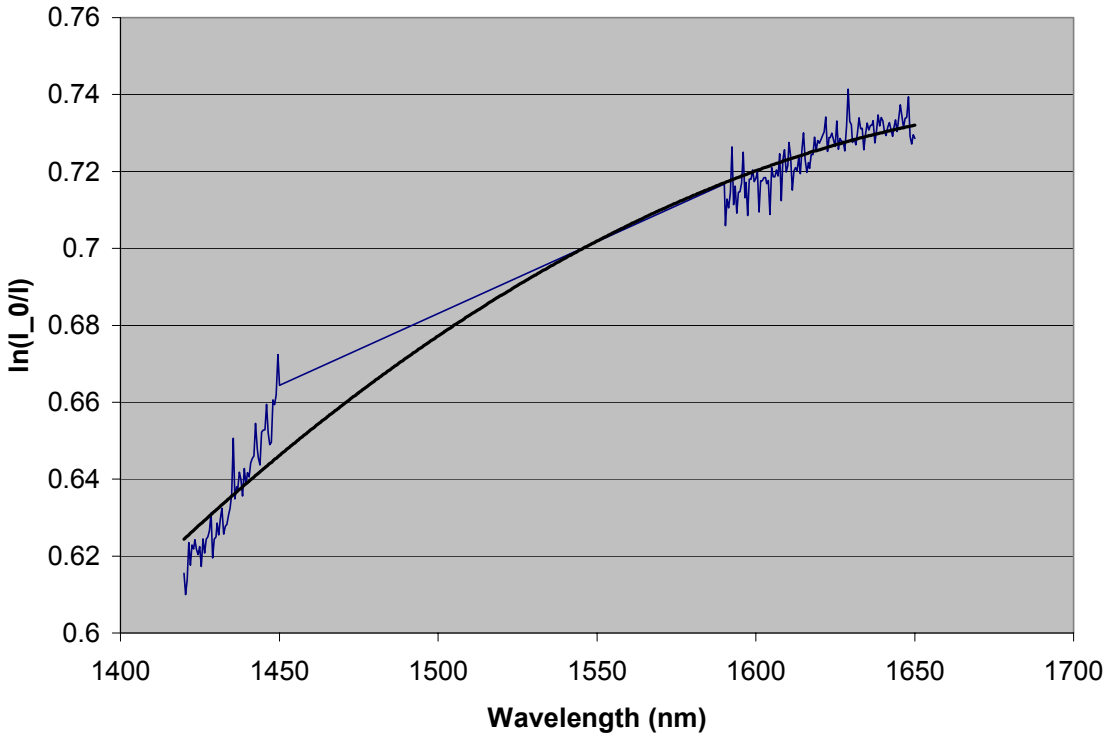

Figure 16: Determining best-fit line from neighboring points
Equation: $y = -1E\text{-}06x^2 + 0.0044x - 3.045$
$R^2 = 0.9804$

Figure 16 shows a quadratic best fit line was used and the equation with the R^2 value appears in the caption. The R^2 value determines how well the line fits the data-points. A value of 1 is perfect, so R^2=0.98 is satisfactory. From the equation obtained, the data in figure 16 is subtracted from the data in figure 15 to normalize the graph. For the final step, the absorption cross section is obtained by the new normalized graph and the ion density per unit volume of the Er:LG22 sample. The values for the Er:L22 sample is a

length of 0.7cm and an N=2.46*10^{20} ion/cm^3. After this step the absorption cross section is obtained and can be viewed in figure 17.

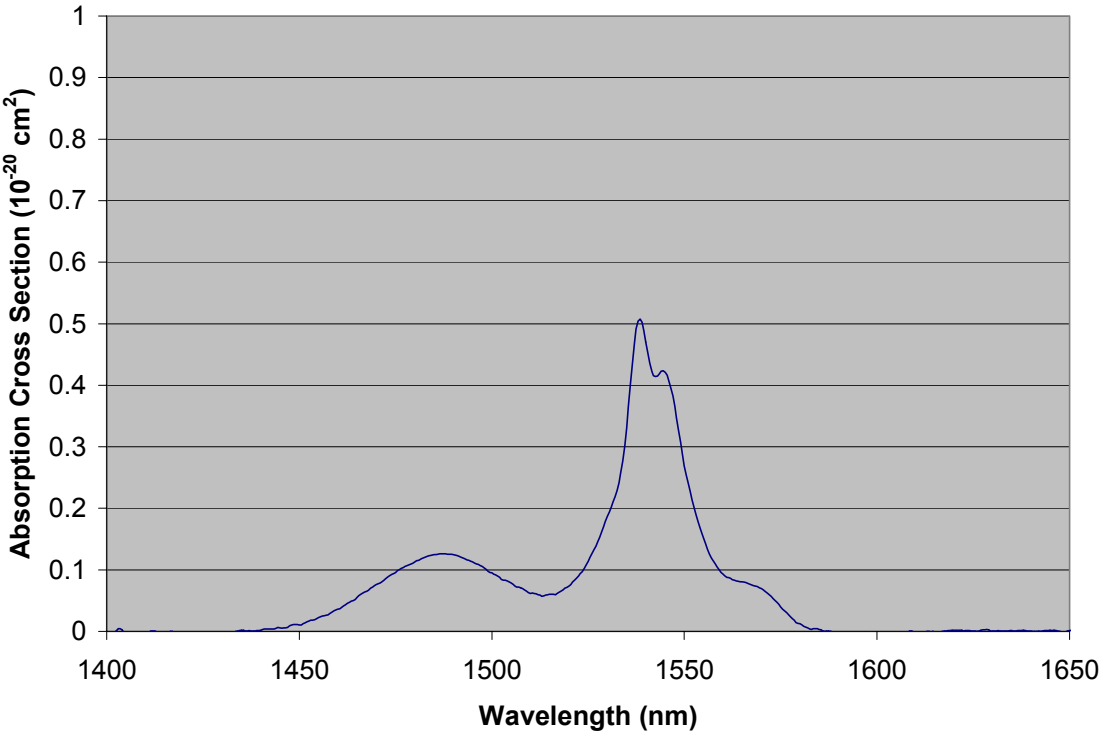

Figure 17: Absorption cross-section of Er:L22 at room temperature

The next step was to enhance peak D (see Figure 11). As mentioned in the background, the method to accomplish this was to use the McCumber Relation (Equation 5). Using this relation a relative emission cross section is obtained, thus enhancing peak D. A constant wavelength (λ_0) had to be chosen, and in the case of this experiment the McCumber relation was normalized using the highest peak of the absorption spectrum (peak B). Therefore any wavelength after peak B of the absorption spectrum in enhanced

and any wavelength before peak B is diminished due to the exponential. The results of this process can be seen in figure 18.

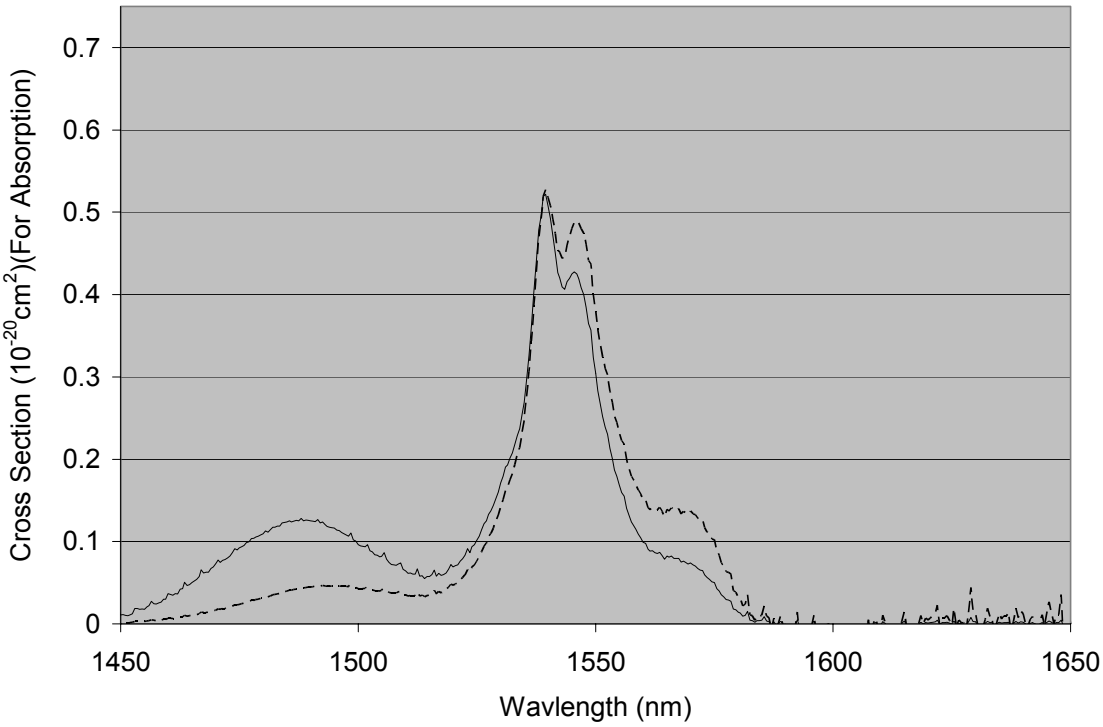

Figure 18: Absorption (solid) and normalized Emission (dashed) Cross-Sections plotted on same graph

The solid line is the absorption cross section; the dashed line is the normalized emission cross section. With the emission cross section it is observed that peak D appears to have more of a well-defined peak; therefore it is more applicable to apply a quadratic fit for the emission spectrum than the absorption spectrum.

Now with an absorption and emission cross section for room temperature the peak values need to be found for A, B, C, and D. A similar method to the best-fit line in Figure 16 was applied. Individual data points were taken around what appeared to be the peak, then a quadratic best-fit line is applied. The reason for this method is that the

signal to noise ratio caused the highest cross section value not always being a peak value. An example can be seen in figure 19 for peak A.

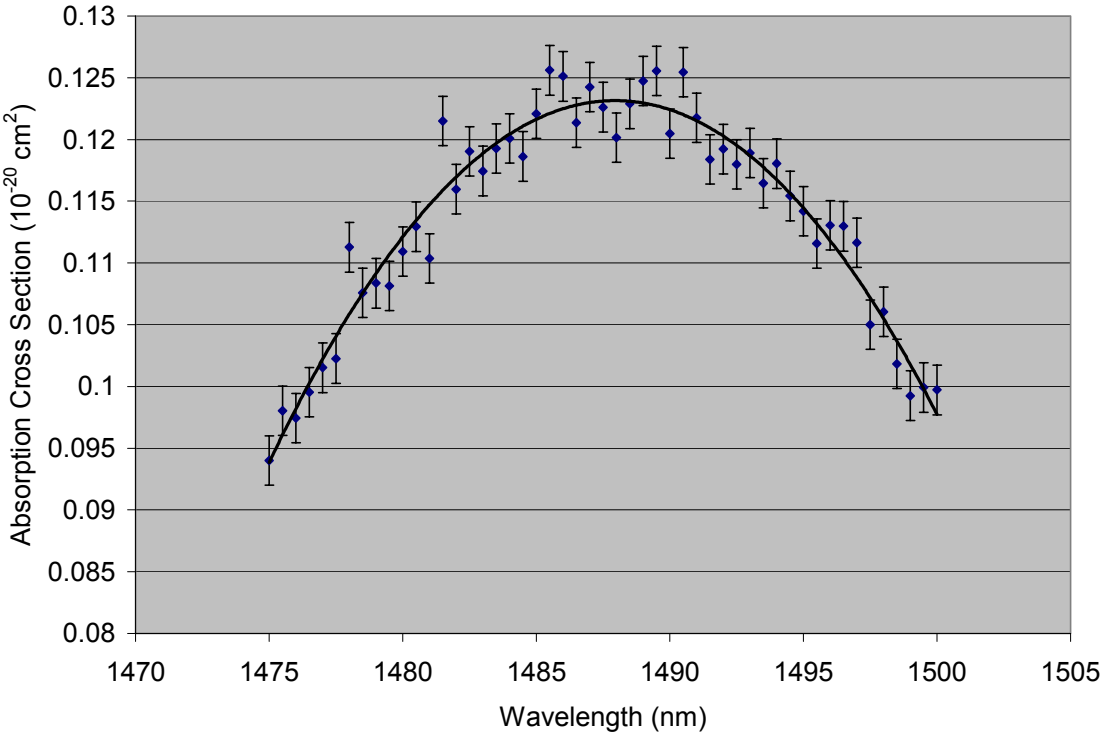

Figure 19: Determining peak value with quadratic fit for Peak A

This procedure is repeated for the remaining peaks B and C. Peak D required a similar method but not as many data points existed for the quadratic fit. An example of peak D can be seen in figure 20.

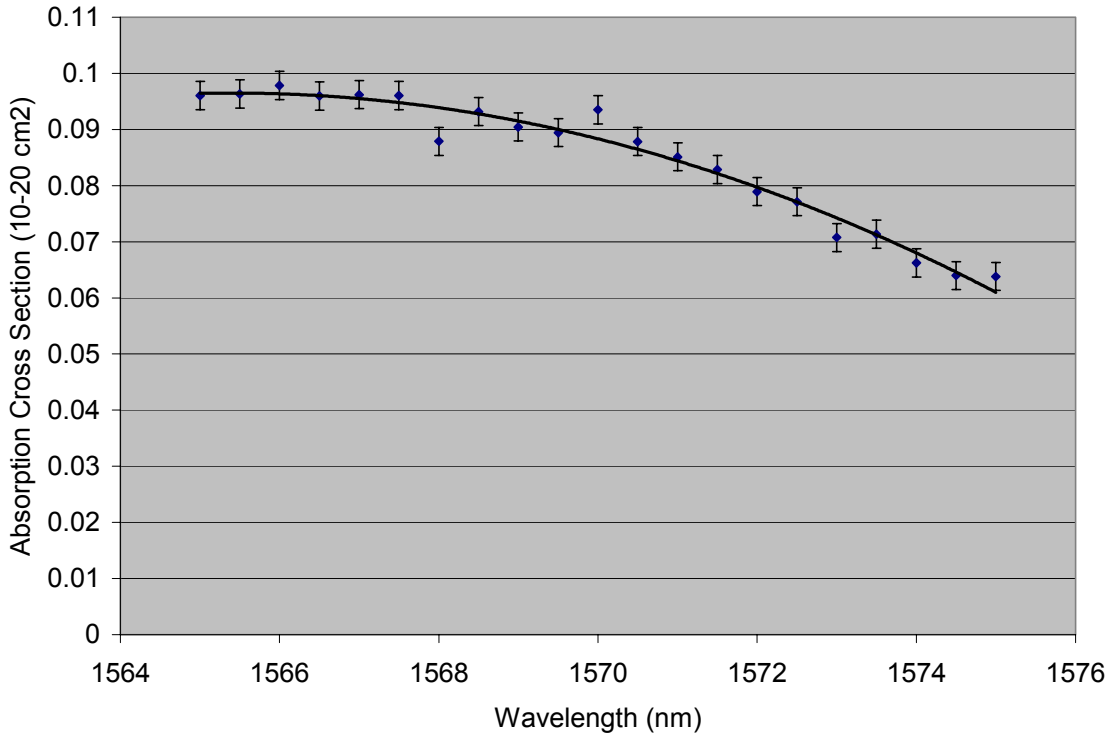

Figure 20: Determining peak value with quadratic fit for Peak D

Compared to Figure 19, Figure 20 does not show a definite peak height. However, an approximate peak height can be determined from the quadratic fit. The peak height value is where the absorption cross section becomes a constant.

After obtaining peak values, the next step is determining the uncertainty in the values. In figures 19 and 20, each data point has an uncertainty. These uncertainties were obtained by repeating the measurement and observing how each individual data point changed. An absolute value of uncertainty for the cross sections was ±0.0025. After finishing the procedure for measurements at room temperature, the experiment was repeated for a number of temperatures by using the hotplate. The data from the experimental absorption and calculated emission cross section are shown in Tables 2 and 3. With the temperature dependence shown in these tables, the data could be analyzed.[11]

Temp (°C)	Absorption Coefficient Peaks (10^{-20} cm^2) A	B	C	D
27	0.1255	0.501	0.427	0.083
58	0.123	0.5035	0.425	0.0905
80	0.1212	0.4848	0.4198	0.0965
106	0.1131	0.4779	0.4068	0.097
128	0.1108	0.4582	0.414	0.1075
170	0.1088	0.4495	0.4063	0.1126

Data of absorption cross-section peaks of various temperatures

Table 2

Temp (°C)	Relative Emission Cross Section Peaks (10^{-20} cm^2) A	B	C	D
27	0.04625	0.501	0.489	0.1387
58	0.0486	0.5035	0.464	0.1445
80	0.052	0.4848	0.464	0.1535
106	0.0518	0.4779	0.45	0.1505
128	0.052	0.4582	0.45	0.16
170	0.05575	0.4495	0.442	0.1671

Data of emission cross-section peaks of various temperatures

Table 3

Analysis and Conclusion

Emission and Absorption Cross-Sections

With the data for peak heights A, B, C, and D for absorption and emission, it is now possible to compare the absolute value of the peak heights and how they changed with temperature as well as ratios of two peak heights and how the ratios vary with temperature.

The first set of data that was examined was the absolute values of peak heights for emission and absorption cross section over the wavelength range of 1400-1600nm. Six different temperatures were recorded for data, but only three were used in Figures 21 and 22 (27 (solid line), 58, 80 (dashed line, 106, 128, 176 (dotted line) degrees Celsius). Figure 21 shows the absorption cross section and how it varies with temperature.

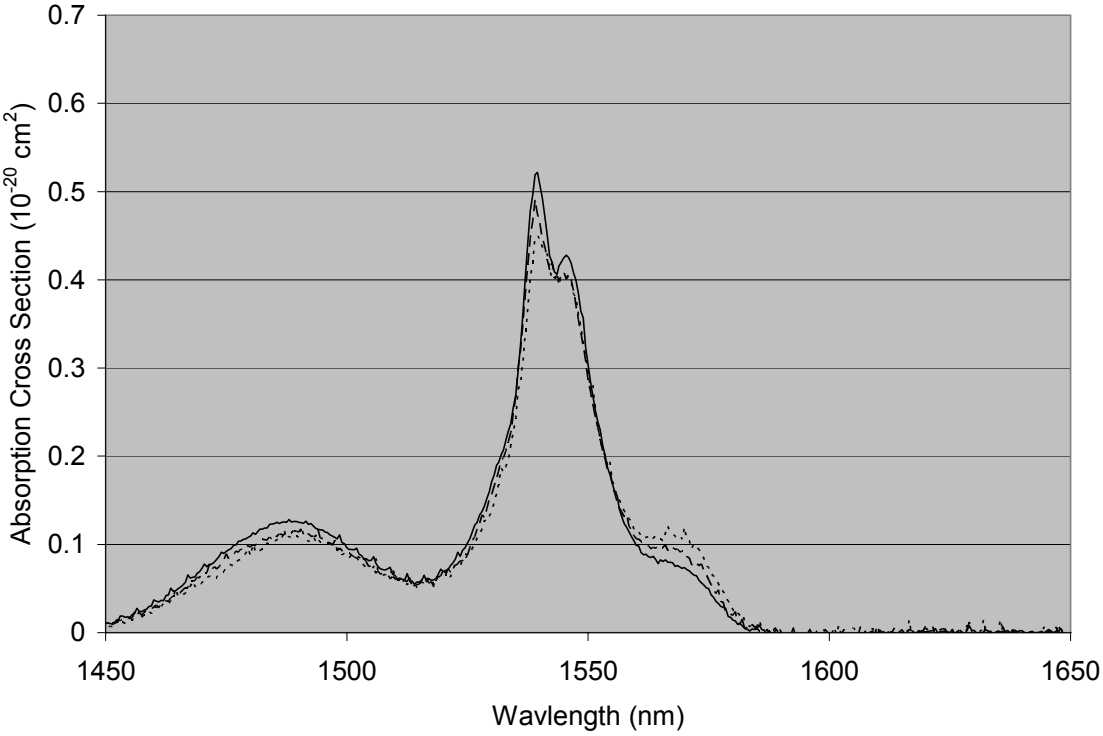

Figure 21: Absorption spectrum observed at 27°C (solid), 80°C (dashed), 176°C (dotted)

From looking at figure 21, it is noticeable that Peak B appears to be effected by temperature change and Peak C appears to experience the least amount of change with temperature. Also as the temperature increased the absorption cross-section value decreased for peaks A, B, and C. But as the temperature increased for peak D, the absorption cross-section began to increase. The same analysis was then conducted on the emission cross section, figure 22.

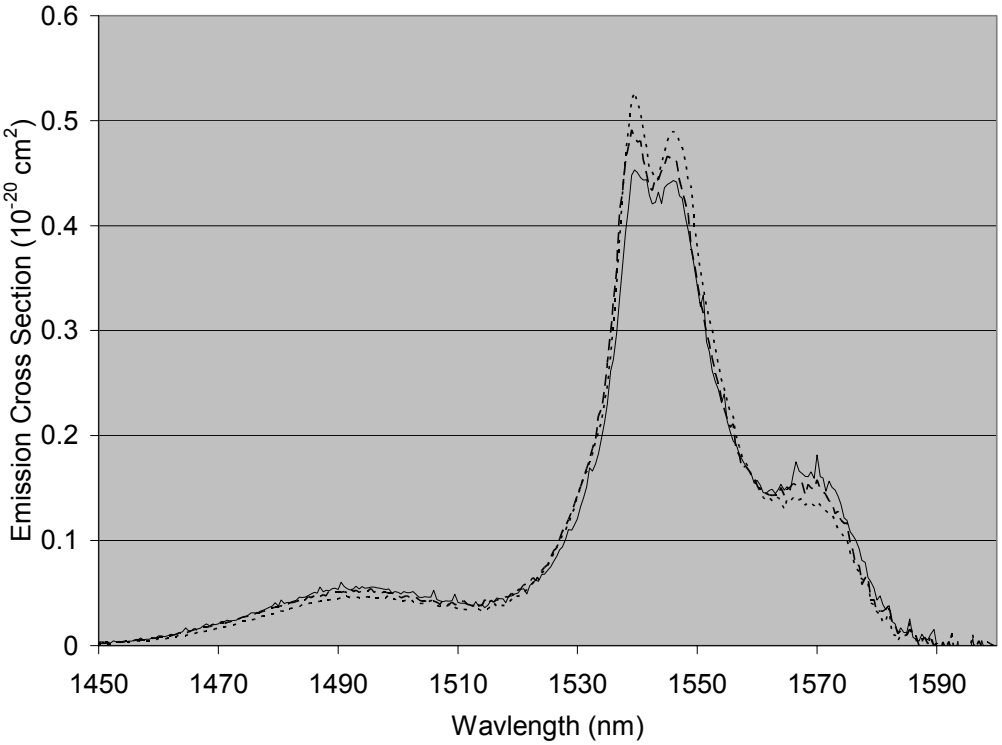

Figure 22: Emission spectrum calculated from absorption at 27°C (dotted), 80°C (dashed), 176°C (solid)

In Figure 22, it is noticeable that for peaks B and C the emission cross-section decreases with temperature. For peaks A and D, the emission cross-section increases with temperature. A similar relationship for emission was found in an article, by Koroshetz, and a figure of his findings can be found in the background as Figure 8.[10]

From Tables 2 and 3, a ratio of the different peak heights was taken and plotted over the temperature interval. The first peak height ratios tested were from the absorption cross section. The ratios of all the peaks were calculated. One example of the graphs plotted is Figure 23

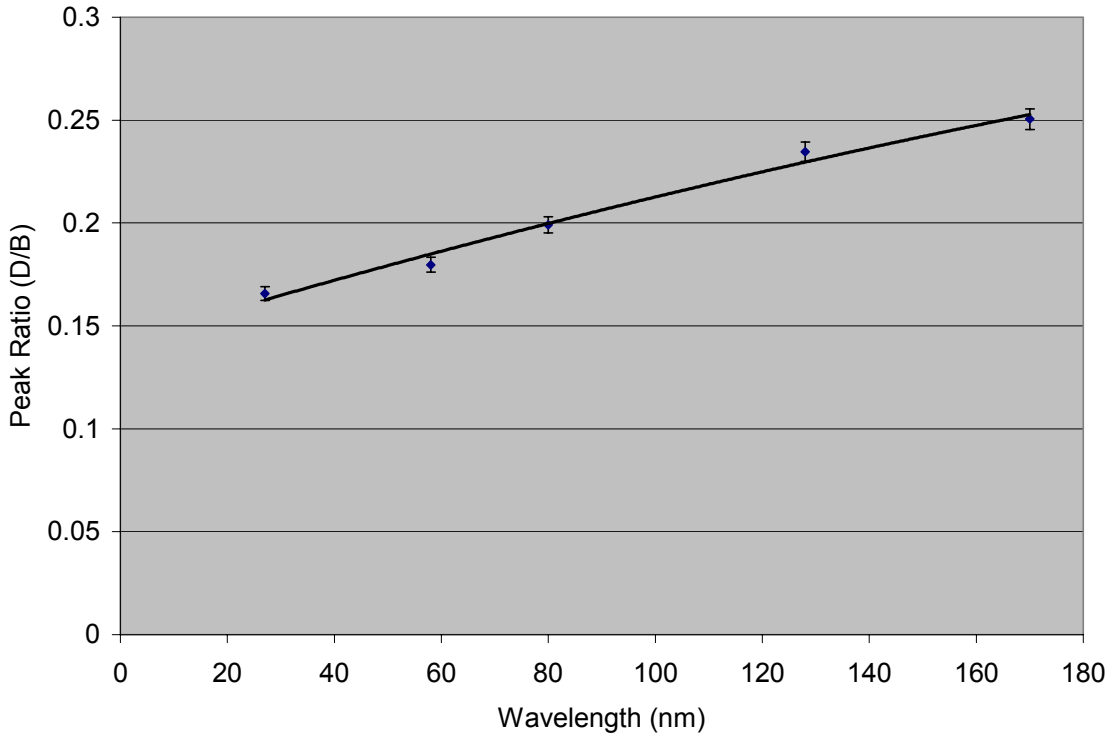

Figure 23: Data plotted from Table 3 Peak Heights (D/B), displayed greatest percentage of temperature change (emission)

Next similar graphs as Figure 23 were created from the data of Table 2. The percentage changes of the absorption cross-section ratio were then calculated as the temperature increased. When peak D was calculated in a ratio with either peak A, B, or C, the change was around 45% with the ratio of D/A showing the greatest amount of change (≈55%). For the ratios excluding D, the percent change was not as great (A/B≈ 4%, B/C≈ 6%). It still shows though peaks B and C experience a greater percent change with temperature than peak A. A graph of for all the peak ratios was created and normalized to a value of 1 at room temperature. The graph in Figure 24-27 shows a clear understanding in which ratios change the greatest as temperature changes. The data for these figures can be viewed in Table 4.

Absorption Cross-Section Normalized Peak Values

Temp (°C)	A	B	C	D
27	1	1	1	1
58	0.980079681	1.00499002	0.995316159	1.090361
80	0.965737052	0.967664671	0.983138173	1.162651
106	0.901195219	0.953892216	0.952693208	1.168675
128	0.882868526	0.914570858	0.969555035	1.295181
170	0.866932271	0.897205589	0.951522248	1.356627

Table 4: Normalized absorption cross-section peak values

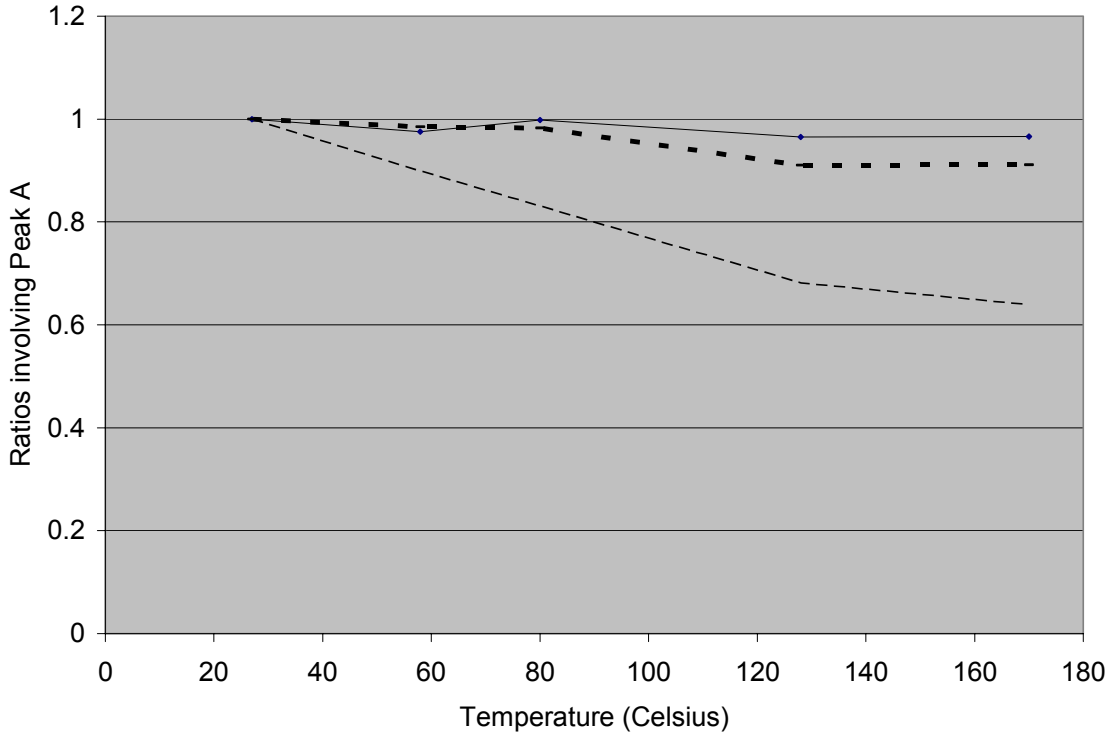

Figure 24: Ratio of peak heights A/B (solid line), A/C (dark dotted line), A/D (dashed line) normalized to room temperature (Absorption)

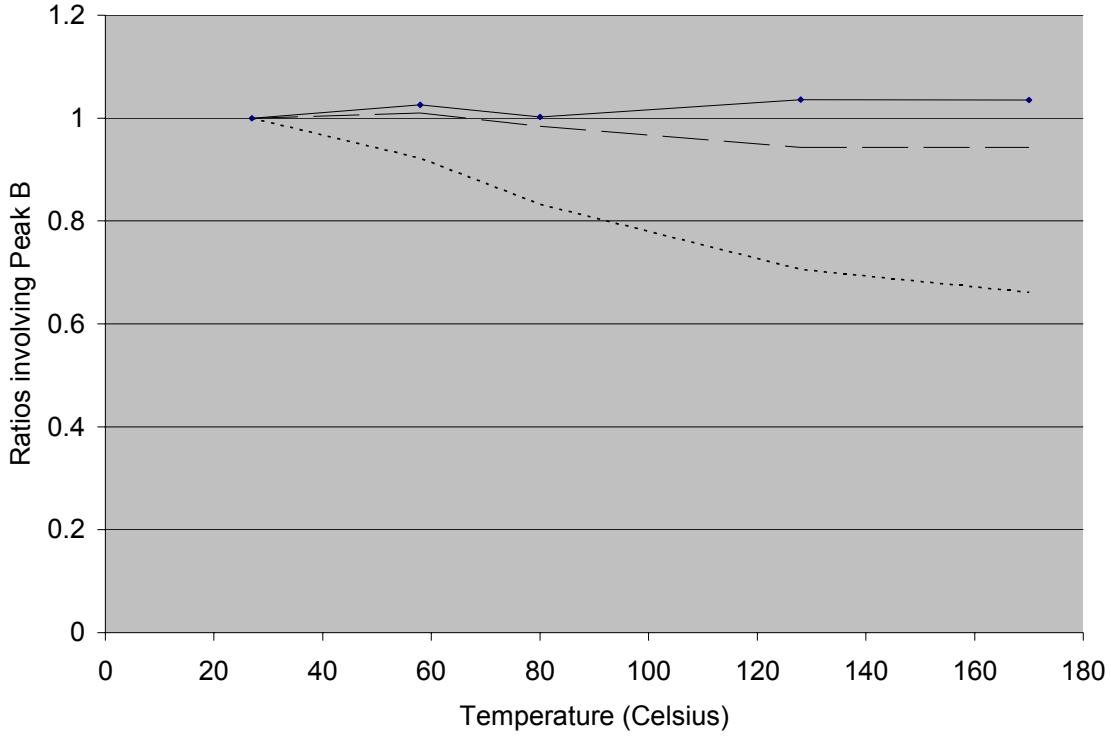

Figure 25: Ratio of peak heights B/A (solid line), B/C (dashed line), B/D (dotted line) normalized to room temperature (Absorption)

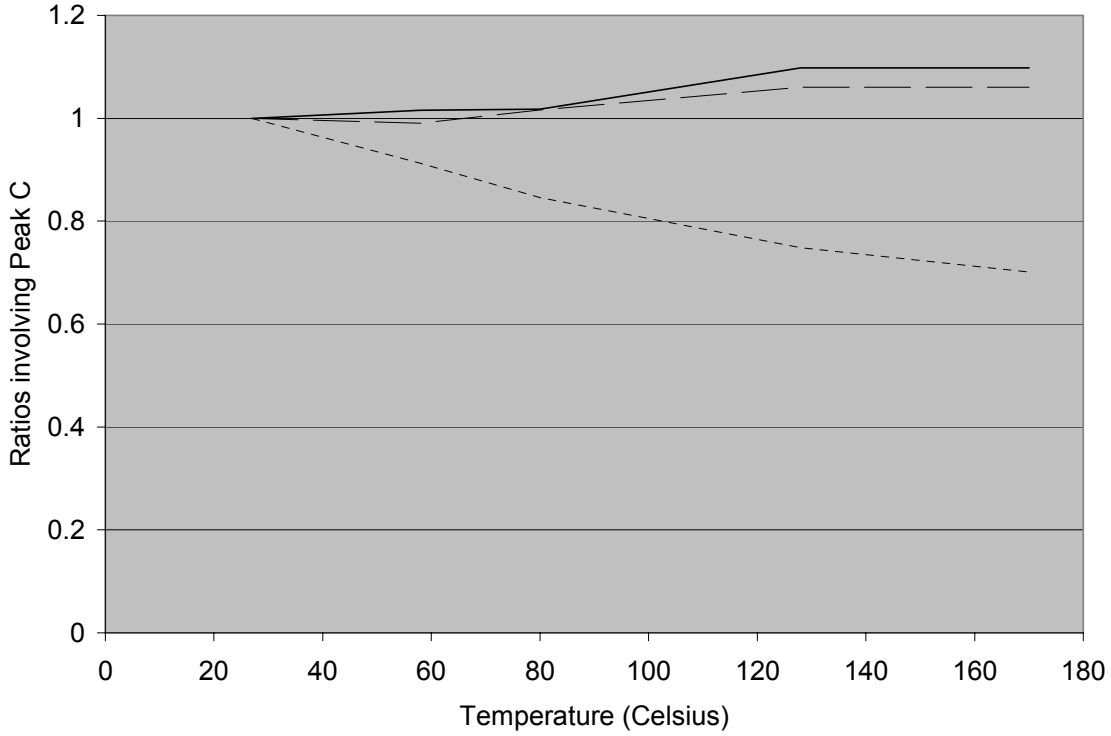

Figure 26: Ratio of peak heights C/A (solid line), C/B (dashed line), C/D (dotted line) normalized to room temperature (Absorption)

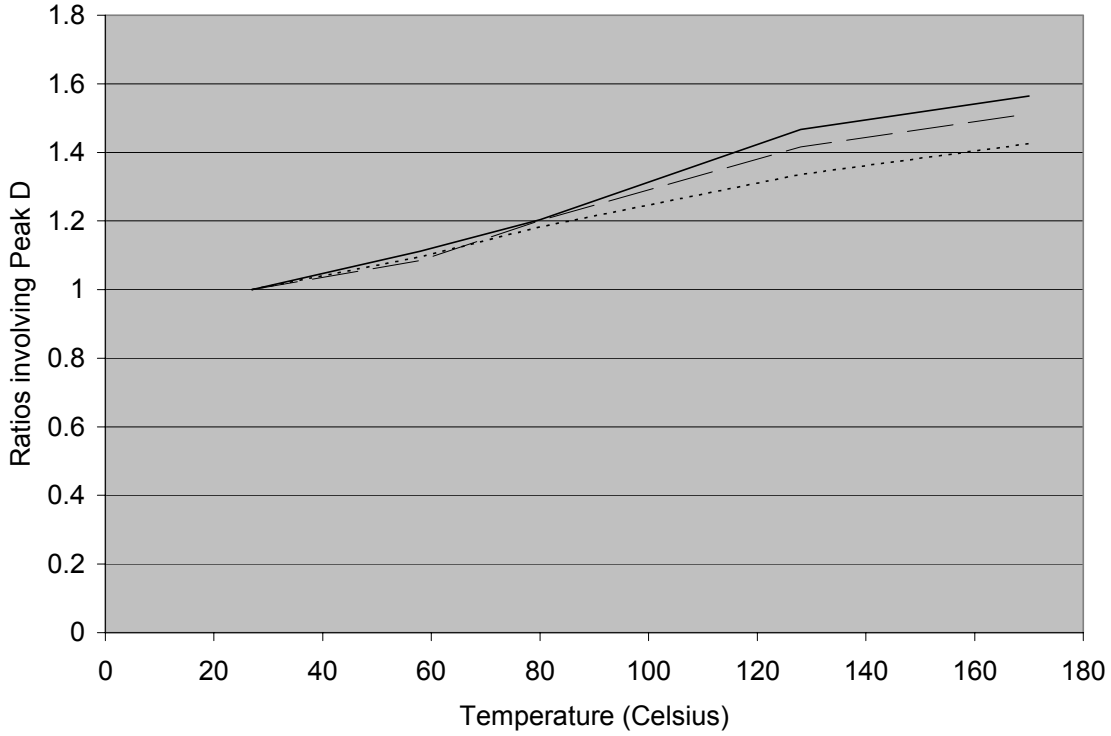

Figure 27: Ratio of peak heights D/A (solid line), D/B (dashed line), D/C (dotted line) normalized to room temperature (Absorption)

The same process was carried out for the emission cross section and results can be seen in figures 28-31. The data for these results can be viewed in Table 5.

Emission Cross Section Normalized Peak Values

Temp (°C)	A	B	C	D
27	1	1	1	1
58	1.050811	1.00499	0.948875	1.041817
80	1.124324	0.967665	0.948875	1.106705
106	1.12	0.953892	0.920245	1.085076
128	1.124324	0.914571	0.920245	1.153569
170	1.205405	0.897206	0.903885	1.204758

Table 5: Normalized emission cross-section peak values

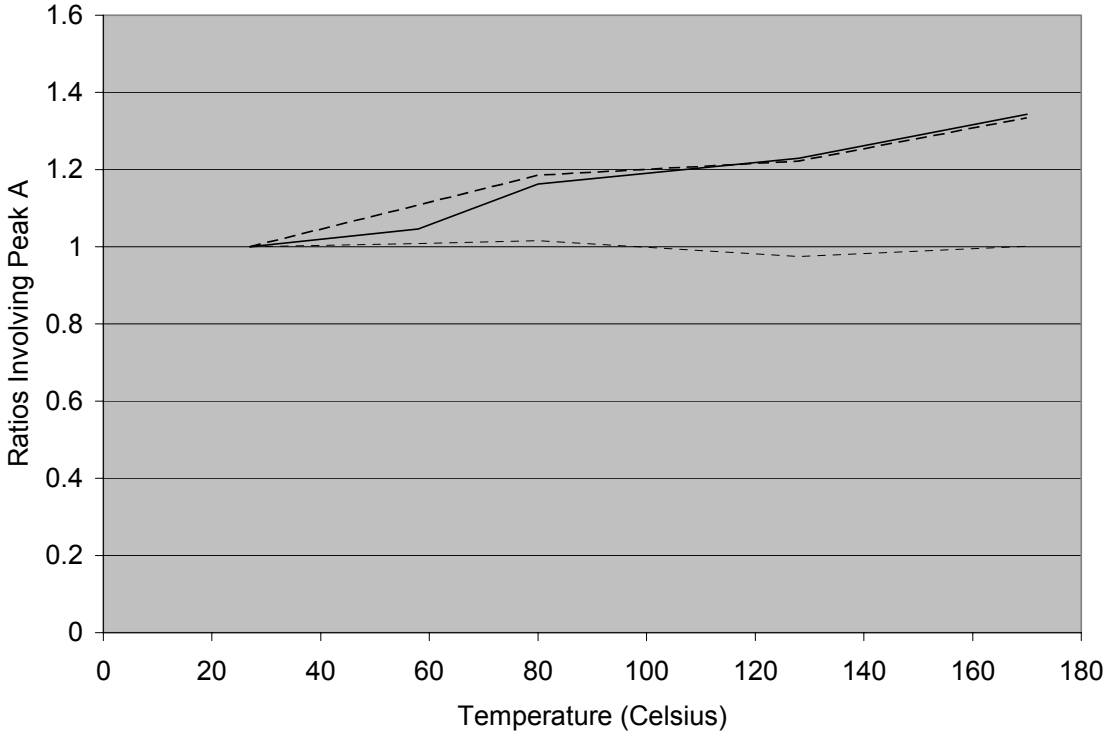

Figure 28: Ratio of peak heights A/B (solid line), A/C (dashed line), A/D (dotted line) normalized to room temperature (Emission)

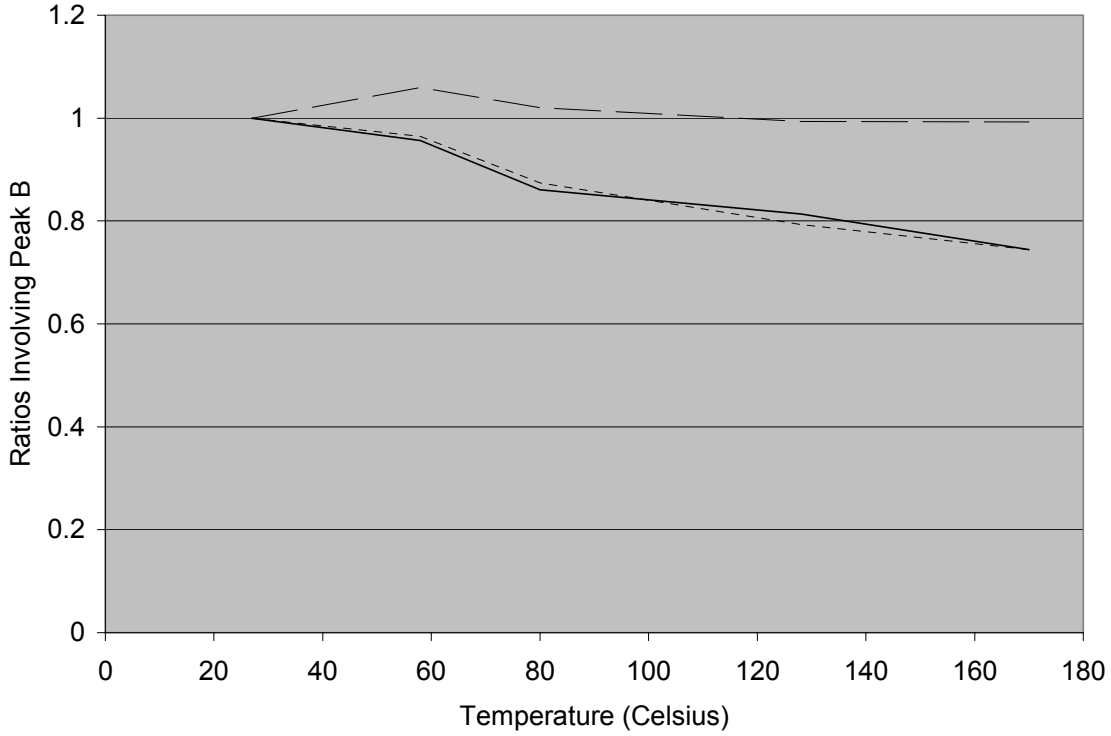

Figure 29: Ratio of peak heights B/A (solid line), B/C (dashed line), B/D (dotted line) normalized to room temperature (Emission)

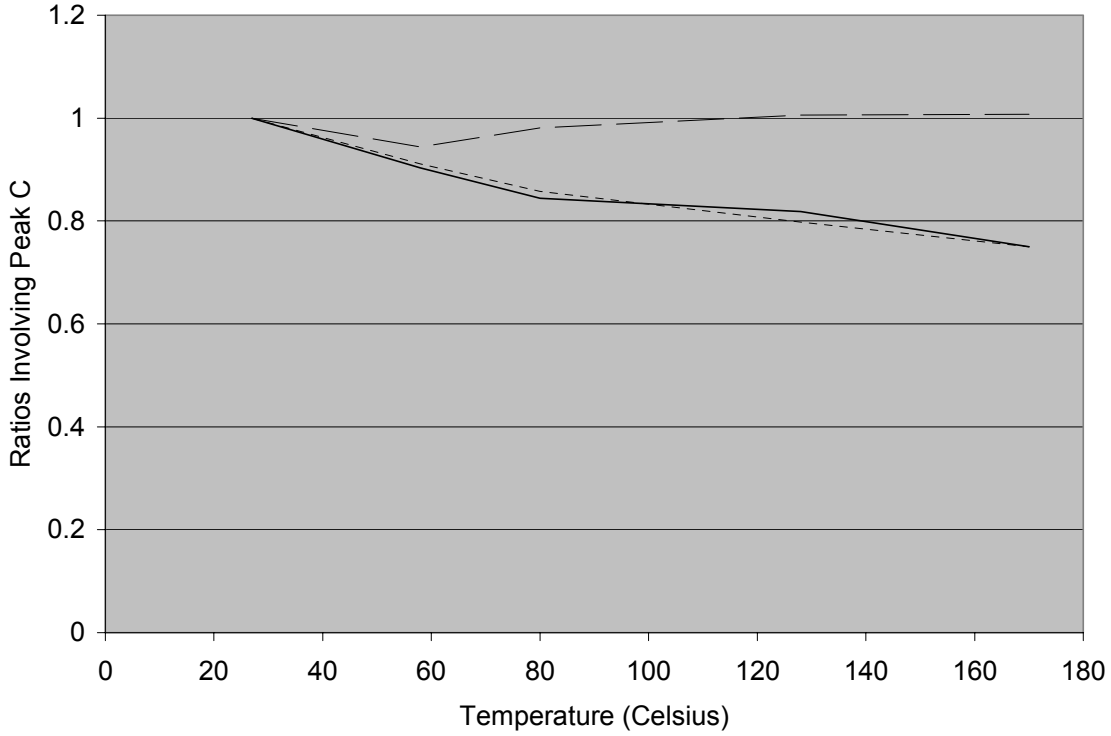

Figure 30: Ratio of peak heights C/A (solid line), C/B (dashed line), C/D (dotted line) normalized to room temperature (Emission)

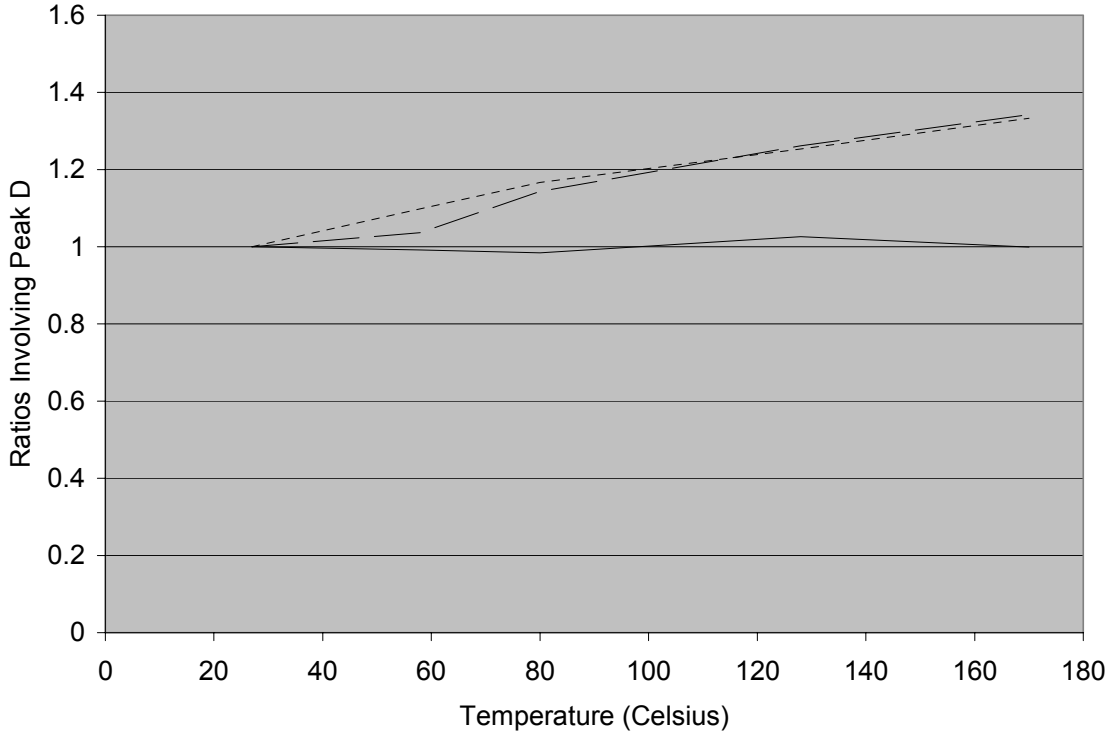

Figure 31: Ratio of peak heights D/A (solid line), D/B (dashed line), D/C (dotted line) normalized to room temperature (Emission)

Precision in Temperature

The non normalized graphs involving the peak ratios were also important in determining the uncertainty in temperature. One example of the graphs is Figure 32.

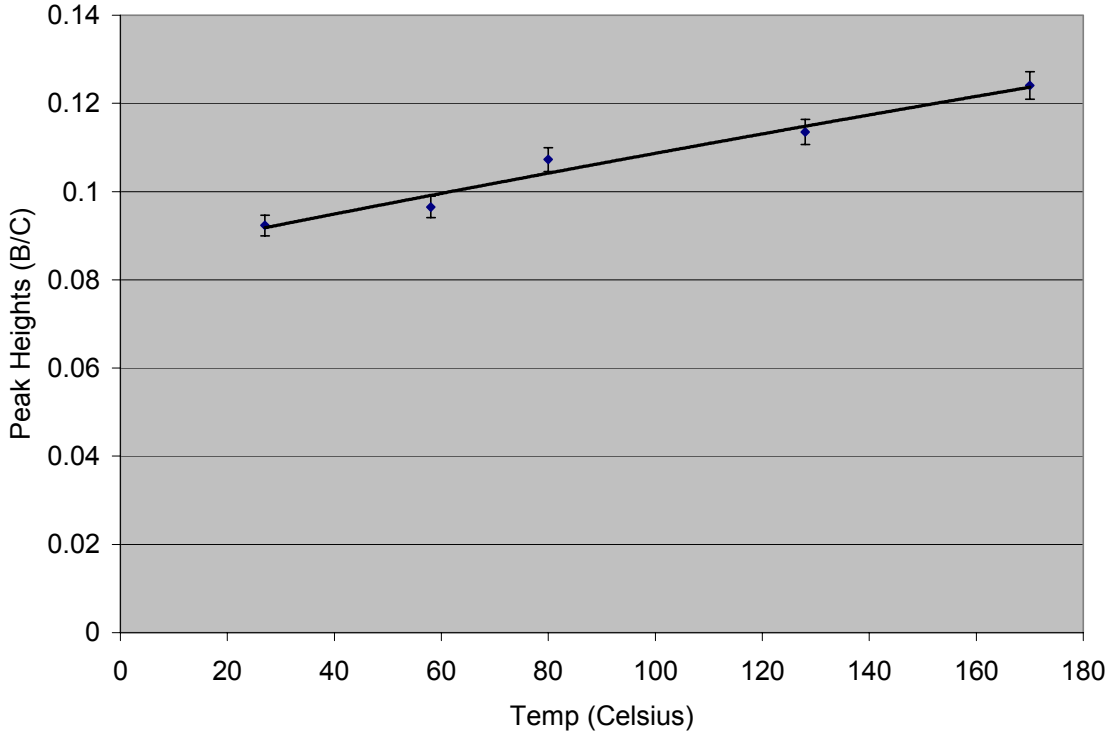

Data plotted from Table 3 Peak Heights (B/C) (Emission)

Figure 32

When determining the ratio of the peak heights, it was also important to understand how to find their uncertainty. Since we are taking the ratio of two cross sections that already have an uncertainty, the uncertainties rule in products and quotients must be used which is[11]

$$\frac{\partial q}{|q|} = \sqrt{(\frac{\partial x}{|x|})^2 + (\frac{\delta z}{|z|})^2} \qquad (9)$$

here q is the ratio, x and z are two of the peaks. By finding their percentage of uncertainty, one is able to then add them together to find the uncertainty for the ratio.[11]

With graphs and uncertainties obtained, it was now possible to determine the uncertainty in temperature. There were two methods in accomplishing this and both provided similar results. The first method was to have a straight best fit line drawn through the data. The equation for this line would be y=Ax+B. The best fit line would have parameters A and B labeled as A_{BEST}, and B_{BEST}. Then two extreme best fit lines could be drawn and the slope and y-intercept could be determined. This then allowed two equations to be determined for A and B

$$A = A_{BEST} + \delta A \tag{10}$$

and

$$B = B_{BEST} + \partial B \tag{11}$$

Figure 33 shows an example of how the lines were determined and drawn on the graph.

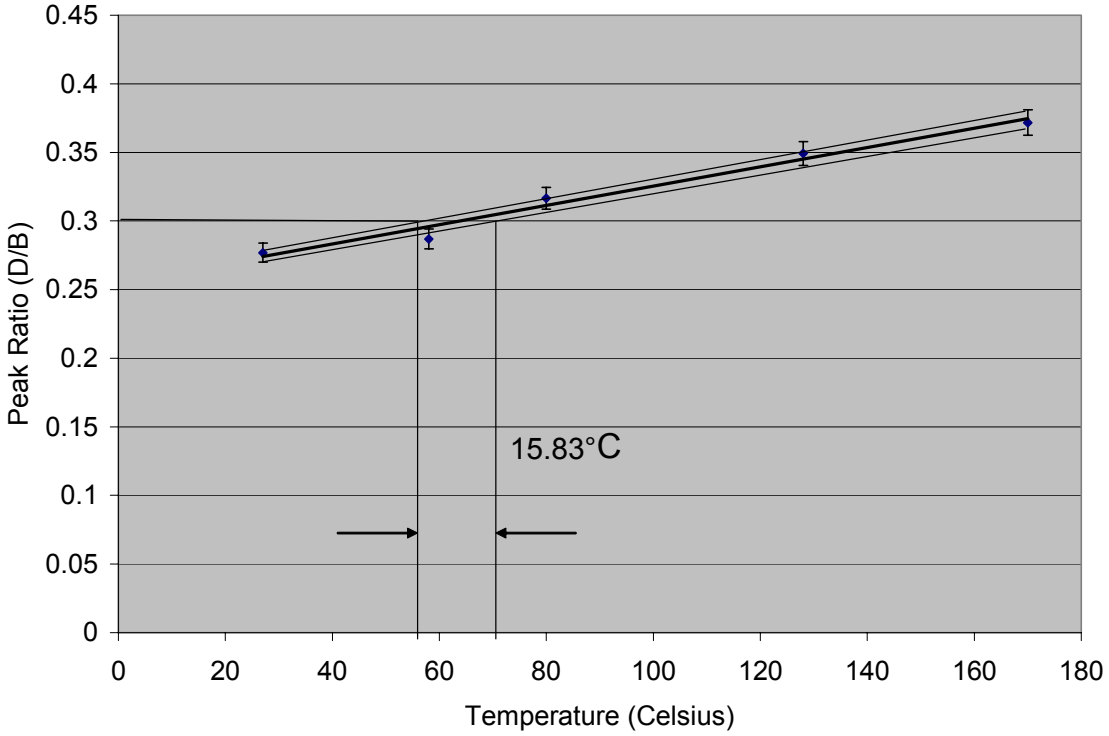

Determining Uncertainty in Temperature with multiple best fit lines

Figure 33

If we pretended to know the ratio of the peaks (D/B) exactly we could determine the uncertainty in the value of x (Temperature). After applying this method an uncertainty of approximately ±7.915K is obtained by pretending the value 0.30 was known. A line was drawn down from this y-value to the corresponding x-value. The difference was then taken between the x-values. This method was then repeated for all the ratios of the absorption cross-section and calculated emission cross-section. The results can be viewed in Table 6. In the article by Nikonorov, their uncertainty in temperature was approximately 5K.[8]

Ratio of Peak Heights (Calculated Emission)		
Peaks	Temp Difference	±(Celsius)
A/B	16.67	8.335
A/C	27.5	13.75
B/A	17.5	8.75
B/D	20.83	10.415
C/A	33.33	16.665
C/D	16.67	8.335
D/B	15.83	7.915
D/C	25	12.5

Table 6: Value for uncertainty in temperature using emission

The other method in obtaining the uncertainty in temperature is using the uncertainties found in the y-direction of peak ratios. These error bars can then be transposed onto the y-axis. Then by drawing a straight line across the graph from the points of uncertainty to the best fit line, a range of temperatures would be found that would correspond to the uncertainty in the y-direction. The value of this uncertainty was found to be approximately 7K for peaks (D/B). The method of obtaining this value can be seen in Figure 34 and values obtained in Table 7.

Ratio of Peak Heights (Calculated Emission)		
Peaks	Temp Difference	±(Celsius)
A/B	20.83	10.415
A/C	28.33	14.165
B/A	19.16	9.58
B/D	23.33	11.665
C/A	30.83	15.415
C/D	20	10
D/B	18.33	9.165
D/C	29.16	14.58

Table 7: Value for uncertainty in temperature using emission

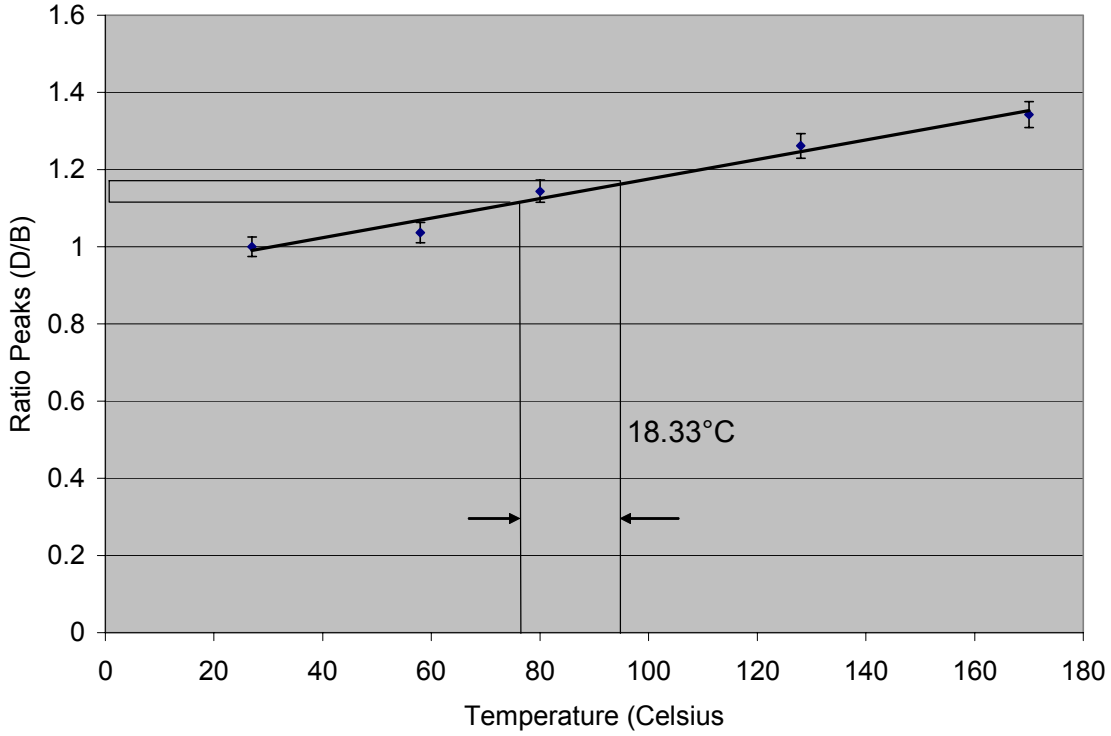

Determining Uncertainty of temperature by using uncertainty in peak heights (D/B)

Figure 34

After comparing all the uncertainties in Tables 6 and 7, it was determined the ratio between peaks (D/B) provided the best ± for uncertainty in temperature.

Stark Level Model

The final part of the project was to predict the Stark levels for the sample Er:L22 using a simplified model. Two models were used for this part of the experiment. The first model was similar to the one by Nikonorov, involving two manifolds, with the lower and upper manifold having two Stark levels. Unlike Nikonorov's model where there were only two transitions, our experiment produced four different transitions at 1494nm, 1539nm, 1545nm, and 1566nm.

From equation 6, once the positions of the Stark levels were determined, it would be possible to determine the energy between these levels. With the Nikonorov model, if correct, the peak energies should be consistent, and the difference between two levels should equal if a similar transition occurs.

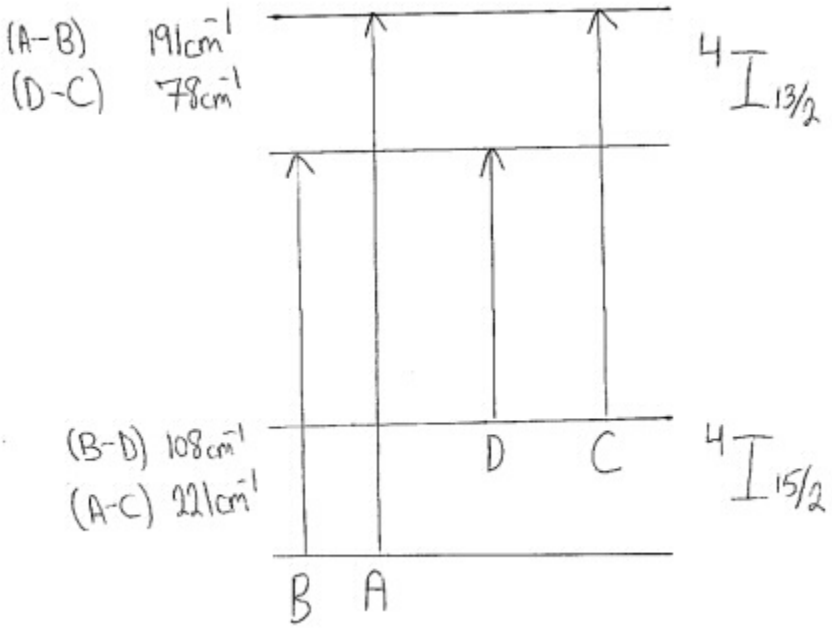

Figure 35: Stark level model of transition peaks between $^4I_{15/2}$ $^4I_{13/2}$ manifolds using Nikonorov's model

Figure 35 shows that the model of two upper and lower level Stark levels is not sufficient. The reason is the energy gaps do not equal one another. The difference between (A-B) and (C-D) should be equal. The same is true with (B-D) and (A-C). Figure 35 gives the values of the photon energies and proves the model by Nikonorov is not suitable for our experiment. Because of this a new model was constructed.

Our new model still consisted of two Stark levels in the higher energy manifold, but now three Stark levels existed for the lower energy manifold. From the previous

model and information obtained, it was concluded that transitions for peaks A and B still occurred on the lowest Stark level for manifold $^4I_{15/2}$. Peak C and Peak D then have to occur on different Stark levels in order to account for the problem in Figure 35.

First the absorption spectrum was examined. By examining Table 4 and 5, it is possible to determine the peak that had the greatest fractional temperature change. For absorption (Table 4 and Figures 24-27), peak D experienced the greatest fractional change of approximately 35.6%. Since peak D showed a stronger dependence on temperature than the other peaks, it was concluded that peak D existed in a higher energy level than the other transitions. Peaks A and B experience approximately the same fractional change as temperature increases for absorption. This observation concluded that peaks A and B would start on the same Stark level in the lower manifold $^4I_{15/2.}$

For emission (Table 5 and Figures 28-31), peak A and D experienced the greatest fractional change of approximately 20.5%, while also peaks B and C experience a similar fractional change of approximately 10%. This observation concluded that peaks A and D involve the same Stark levels in the upper manifold, and peaks B and C involve another common Stark level in the upper manifold.

Another key piece of information was peak D experienced opposite changes (as seen in Figures 21 and 22 for absorption and emission respectively) than peaks B, and C as the temperature increased. When looking at the photon energies and Stark levels in the background articles by Nikonorov[8] and Koroshetz[10], a similar observation was made. The Stark levels that were determined from their study, was the transition started at the highest Stark level for $^4I_{15/2}$ and travel to upper manifold $^4I_{13/2}$. This can be seen in figure

5.[8] As in Figure 35, it was important in the new model for the energy gaps to be consistent. Our proposed model is shown in Figure 36.

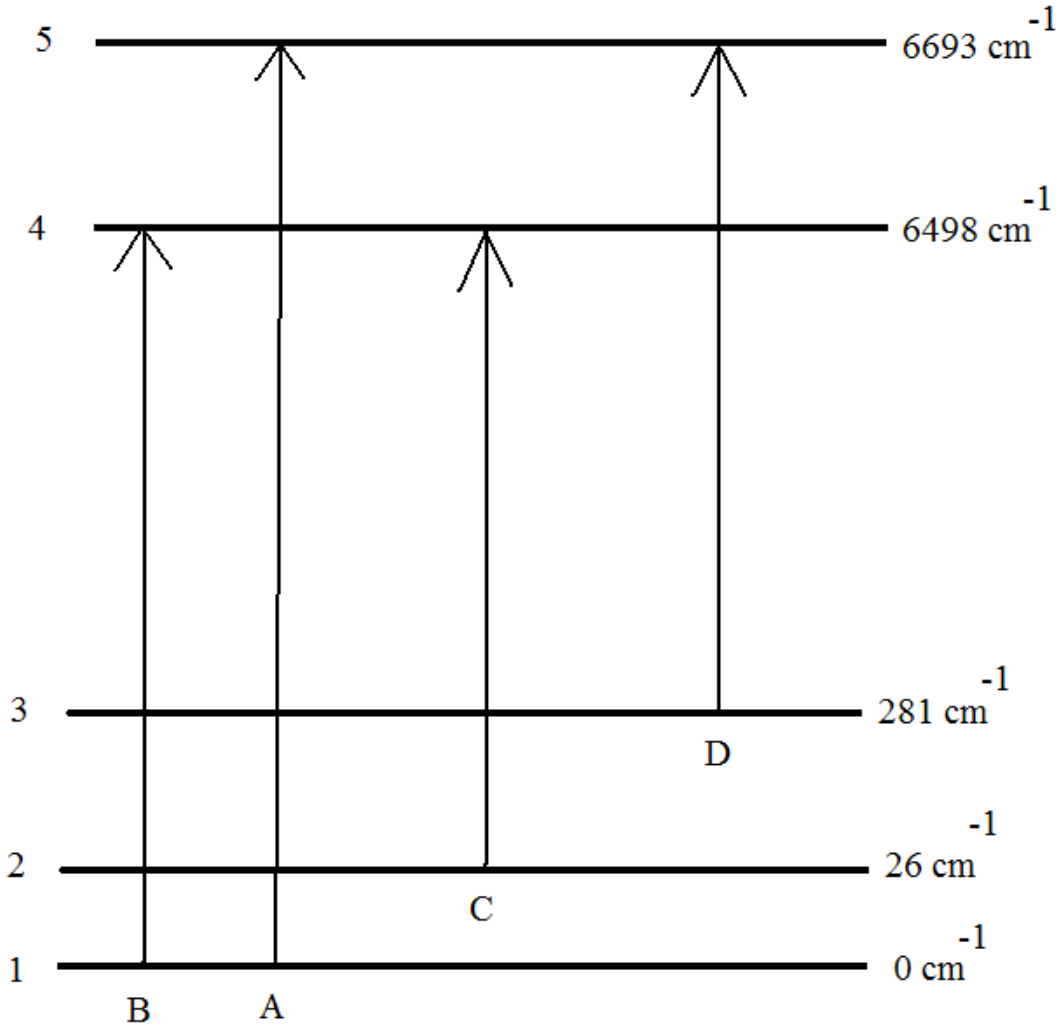

Figure 36: Stark level model of transition peaks between $^4I_{15/2}$ $^4I_{13/2}$ manifolds (Data taken from Table 1 for Absorption)

When comparing the model in Figure 36 with the obtained data, it appears to be consistent. To confirm that the model is correct the Boltzmann factor was calculated for the energy difference between the levels. The Boltzmann factor (equation 2) shows the

probability of atoms per unit volume existing in the lower and upper energy levels when compared to the energy gaps. When calculating the Boltzmann factor between two energies levels, we are able to prove that Figure 36 is consistent with previous figures. First we will look at Energy level 1 and 2. The Boltzmann factor at room temperature for these levels is approximately 0.878. As temperature increases the Boltzmann factor will not increase greatly because E_2-E_1<<kT. A small Boltzmann factor change explains why the two energy levels have a small energy gap between the Stark levels. For absorption cross-section, when looking at peaks A and B (Figure 21), as temperature increases, the absorption cross-section decreases. The Boltzmann factor explains that as the temperature increases, the atoms would move to the upper Stark levels, thus decreasing the absorption cross-sections. Therefore it is reasonable to place peaks A and B on the lowest Stark level in the lower manifold. The Boltzmann factor for the energy gap between levels 3 and 1 will be greater than E_2-E_1 because E_3-E_1>kT. Peak D is the most temperature dependent of all the peaks therefore would originate in the third Stark level for the lower manifold.

Next the emission cross-section (Figure 22) was examined. For peaks A and D, as the temperature increases, the emission cross-section increases. The Boltzmann factor explains that for emission the atoms should exist primarily in the lowest Stark level for the upper manifold. However, as the temperature increases, the emission cross-section originating from the higher Stark level should increase because of the increasing Boltzmann factor. In the case of peaks A and D, they change by the same fractional percentage as seen in Figure 28-31. As temperature increases for peaks B and C, the

emission cross-section decreases, as expected from the decreasing population in the lowest Stark level for the upper manifold.

In conclusion, while the results of obtaining the best uncertainty of ±9K and ±7K (ratio of D/B) may be useful in some situations, it probably will not be for accurate measurements. It is possible to improve upon this approach by increasing the signal to noise ratio. This can be accomplished by a number of methods. One way is to upgrade the equipment as technology continues to improve upon the signal to noise ratio. Another way is to run a slower scan multiple times. As more scans are recorded, the noise in data becomes less noticeable. For the Stark levels, the data manipulated in a way that told which peak in came from which Stark level. Overall work can be continued in the future to expand upon this process as technology continues to advance and the signal to noise ratio is improved upon.

---

[1] Freedman, Young. Univeristy Physics with Modern Physics. Addison Wesley: 2004.
[2] Digonnet, Michael J. Rare Earth Doped Fiber Lasers and Amplifiers. Marcel Dekker: 1993.
[3] Quimby, Richard S. Photonics and Lasers. Wiley: 2006.
[4] Yoshioka, Daijiro. Statistical Mechanics. Springer: 2007.
[5] Griffiths, David J. Introduction to Quantum Mechanics. Prentice Hall: 2007.
[6] Aggarwal, Lu. Fluoride Glass Fiber Optics. Academic Press: 1991.
[7] Martin, Rodica M. WPI PhD Thesis: Reciprocity between Emission and Absorption for Rare Earth Ions in Glass. 2006.
[8] Nikonorov, Przhevuskii, Lunter. "Effect of heating on spectral characteristics of Er-doped laser glasses". Proc. SPIE Vol. 3622, January 1999, p. 144-152.
[9] Zemon, Andrews, Miniscalco, Hall, Wei, Folweiler. "Characterization of Er^{3+}-doped Glasses by Fluorescence Line Narrowing". Journal of Applied Physics. Volume 69, Issue 10. May 1991 pgs. 6799-6811.
[10] Koroshez, Brickeen, Fahr, Rapaport, Bass. "Athermal Emission in Yb, Er Glass." Optics Express Vol. 15 Iss. 18, (2007). pgs. 11530-11535.
[11] Taylor, John R. introduction to Error Analysis. University Science Books: 1982.